

# Ecotoxicity and Sustainability of Emerging Pb-Based Photovoltaics

Xingwen Lu, Dong Yan, Jiangtao Feng, Meng Li,\* Bo Hou,\* Zhe Li,\* and Fei Wang\*

Emerging Pb-based photovoltaic (PV) technologies, including in particular solution processed halide perovskite solar cells (PSCs) and Pb chalcogenide quantum dot solar cells (QDSCs), are among the most promising next-generation PV technologies for a range of disruptive energy and electronic applications. However, the potential toxicity and leakage of hazardous Pb species have become one of the main barriers to their large-scale application. When solar cells are subject to physical damage or failure of encapsulation, rapid leakage of Pb may occur, which can be accelerated by exposure to external environmental weathering conditions such as rainfall and elevated temperature. Herein, an in-depth investigation on the essential role of Pb in PSCs and QDSCs, as well as common causes of Pb leakage, is undertaken. The hazardous effects of Pb toxicity on soil plants, bacteria, animals, and human cells are also evaluated. Recent progress in developing effective strategies for Pb leakage reduction, such as Pb-free or Pb-less perovskite materials, device architecture design, encapsulation absorbers for PSCs, and core-shell structure and ligand exchange method for QDSCs, in addition to Pb recycling strategies of end-of-life solar cells are summarized. This review provides quantitative insights into the future development of eco-friendly emerging Pb-based PV technologies.

excitation, and transport ability.<sup>[1–5]</sup> In just a few years, it has achieved a power conversion efficiency (PCE) of over 25.7%, comparable to silicon PVs.<sup>[6–9]</sup> While Pb-based PSCs exhibit exceptional promise for mass production,<sup>[10–12]</sup> there are growing concerns about their environmental impact due to the potential toxicity and leaching of harmful Pb species throughout their lifetime.

Colloidal quantum dots (QDs) are another promising candidate for the next-generation PV application, which has received enormous attention because of the excellent optical and electronic properties enabled by their unique size-dependent quantum confinement.<sup>[13–15]</sup> Pb chalcogenide QDs (e.g., PbS, PbSe) are among the most promising nanoparticle (NP) materials in PVs, with certified PCEs as high as 13.8% in PbS QDSCs.<sup>[16,17]</sup> The low-cost and scalable solution-based processing methods can offer QDs a wide range of bandgaps, and generally better stability

than organic chromophores. Despite the continuously increasing PCEs of QDSCs, device stability remains a significant challenge for industrial applications. Beyond PV, QDs have further demonstrated their promising application in biomedical imaging, display and electronics industries. Similar to Pb-based PSCs, growing concerns also arise from their potential Pb<sup>2+</sup> toxicity,

## 1. Introduction

Metal halide perovskite solar cells (PSCs) are established as a highly promising next-generation photovoltaics (PVs) technology due to their superior optoelectronic properties, such as high light absorption coefficient, long carrier diffusion length, high carrier

X. Lu  
School of Environmental Science and Engineering  
Institute of Environmental Health and Pollution Control  
Guangdong University of Technology  
Guangzhou 510006, China

D. Yan  
Guangdong-Hong Kong-Macao Joint Laboratory for Intelligent Micro-Nano Optoelectronic Technology  
School of Physics and Optoelectronic Engineering  
Foshan University  
Foshan 528225, China

 The ORCID identification number(s) for the author(s) of this article can be found under <https://doi.org/10.1002/solr.202200699>.

© 2022 The Authors. Solar RRL published by Wiley-VCH GmbH. This is an open access article under the terms of the Creative Commons Attribution License, which permits use, distribution and reproduction in any medium, provided the original work is properly cited.

DOI: 10.1002/solr.202200699

D. Yan, M. Li, Z. Li  
School of Engineering and Materials Science (SEMS)  
Queen Mary University of London  
London E1 4NS, UK  
E-mail: zhe.li@qmul.ac.uk

J. Feng  
Department of Environmental Science and Engineering  
State Key Laboratory of Multiphase Flow in Power Engineering  
School of Energy and Power Engineering  
Xi'an Jiaotong University  
Xi'an 710049, China

M. Li  
Key Lab for Special Functional Materials of Ministry of Education  
National & Local Joint Engineering Research Center for High-efficiency Display and Lighting Technology  
School of Materials Science and Engineering  
Collaborative Innovation Center of Nano Functional Materials and Applications  
Henan University  
Kaifeng 475004, China  
E-mail: mengli@henu.edu.cn

which may pose a threat to the environment and human health.<sup>[18]</sup>

Pb is a toxic metal with natural concentrations of 12–20 ppm in bedrock and soils and 0.03  $\mu\text{g L}^{-1}$  in stream water.<sup>[19]</sup> Available data from the International Lead and Zinc Study Group estimated that Pb consumption was up to 12 205 000 tons in 2021, owing to the advantages of its low cost, malleability, high density, low melting point, and high corrosion resistance.<sup>[20]</sup> With the rapid growth of the PV market, the global cumulative solar capacity reached about 773.2 GW in 2020.<sup>[21]</sup> If 1 GW of solar PV capacity using perovskite solar panels with an efficiency of  $\approx 25\%$  containing  $\approx 3.5$  tons of lead with a 0.5  $\mu\text{m}$  thick Pb-based perovskite layer,<sup>[22,23]</sup> the total amount of Pb contained in PSCs is  $\approx 541$  tons assuming only 20% of 773.2 GW PV market is occupied by perovskite solar panels.<sup>[21]</sup> Therefore, a sustainable strategy is an essential prerequisite to handling and disposing of Pb-based perovskite materials to effectively mitigate the risk of  $\text{Pb}^{2+}$  leakage.

The widespread consumption of Pb-based PSCs and QDSCs may induce a severe impact on the environment if no effective Pb management strategies are implemented. U.S. Environmental Protection Agency (EPA) regulates the upper limit of Pb concentrations in drinking water and air are 15  $\mu\text{g L}^{-1}$  and 0.15  $\mu\text{g m}^{-3}$ , respectively. The Ministry of Ecology and Environment (MEE) of China stipulates that maximum allowable Pb contents in drinking water and air are 10  $\mu\text{g L}^{-1}$  and 0.5  $\mu\text{g m}^{-3}$ , respectively. In addition, the European Union's Restriction of Hazardous Substances (RoHS) allowed maximum concentration for Pb is 0.1% by weight in homogenous materials of the electronic device. However, it is worth noting that the use of Pb in some installed solar cells (e.g., PSCs of glass substrates) is exempt from this regulation.<sup>[24]</sup>

It is widely established that halide perovskite materials can be vulnerable to degradation in outdoor conditions, such as exposure to moisture/water, ultraviolet light, damp heat, and oxygen, especially upon physical damage or failure of encapsulation.<sup>[25]</sup> Toxic and soluble Pb species can leak out of Pb-based PSCs and QDSCs, posing a severe threat to the surrounding environment. The potential environmental impact of PSCs and QDSCs due to the contamination of  $\text{Pb}^{2+}$  to groundwater, soil, and air, in addition to the subsequent impacts on soil plants, bacteria, animals, and human cells have been widely investigated.<sup>[20,26–33]</sup> The leaching behavior of  $\text{Pb}^{2+}$  from perovskite films or devices under controlled environmental conditions, including heavy rainfalls, high humidity, hail, rainfall temperature, and intense sunlight has been investigated.<sup>[26,27,30–32,34–36]</sup> Multiple strategies were developed to mitigate  $\text{Pb}^{2+}$  leakage while maintaining the performance of PSCs, including the development of Pb-free or

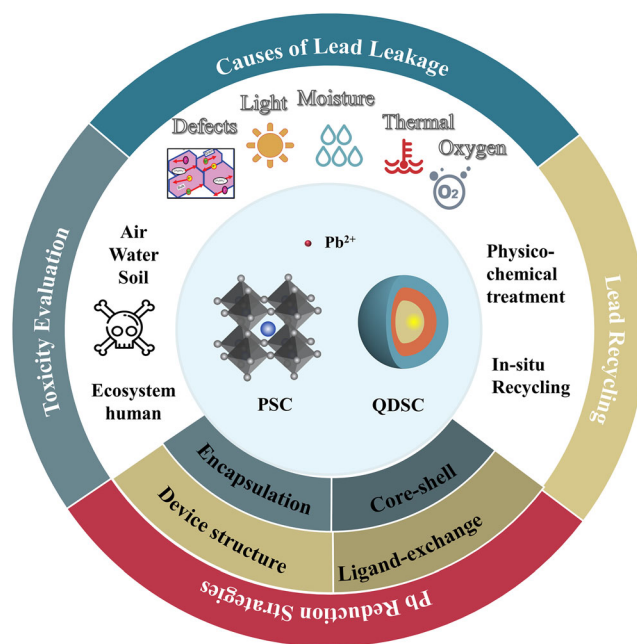


**Figure 1.** Schematic of contents.

Pb-less alternatives to Pb halide perovskites, Pb-absorbing materials, novel device structures, and encapsulation methods. For the toxicity reduction of QDSCs, core-shell structure and ligand exchange method are discussed. Furthermore, Pb recycling methods were also developed to mitigate the environmental impacts of PSCs beyond their lifespan. Some recent reviews have provided one or some of the abovementioned aspects in Pb management of PSCs,<sup>[21,37,38]</sup> while a comprehensive review of Pb management of emerging Pb PVs is still lacking within the community. As a result, it is important to account for the development and provide insights for the environmental impact assessment,  $\text{Pb}^{2+}$  leakage mitigation, and recycling toward their large-scale commercialization.

As shown in **Figure 1**, this review discusses the critical role of Pb in PSCs and Pb-based QDSCs, the causes of  $\text{Pb}^{2+}$  leakage, the leaching behavior of  $\text{Pb}^{2+}$  from PSCs and QDSCs to air, soil, and groundwater under weather conditions of heavy rain and high temperature. The negative influence of  $\text{Pb}^{2+}$  toxicity on soil plants, bacteria, animals, and human cells is systematically analyzed. The strategies for mitigation of  $\text{Pb}^{2+}$  leakage and novel recycling methods are thoroughly discussed. This review highlights effective strategies for reducing  $\text{Pb}^{2+}$  leakage, especially in the development of novel structure design, encapsulation methods, and Pb-absorbing materials.

## 2. The Role of Pb in Emerging Pb-Based PVs

### 2.1. The Critical Role of Pb in PSCs

Perovskite materials possess superior optical and electronic properties, such as optimal energetic bandgap, high light absorption coefficient ( $\approx 10^5 \text{ cm}^{-1}$ ), long carrier diffusion length (up to 1  $\mu\text{m}$ ), high carrier mobility (electron 7.5  $\text{cm}^2 \text{ V}^{-1} \text{ s}^{-1}$ , hole 12.5  $\text{cm}^2 \text{ V}^{-1} \text{ s}^{-1}$ ), small exciton binding energies, only

B. Hou  
School of Physics and Astronomy  
Cardiff University  
Cardiff, Wales CF24 3AA, UK  
E-mail: hou6@cardiff.ac.uk

F. Wang  
School of Environment  
Guangdong Key Laboratory of Environmental Pollution and Health  
Jinan University  
Guangzhou 510632, P. R. China  
E-mail: wf1984@jnu.edu.cn

12.6 meV Urbach energy, and high tolerance to defects with trap densities of  $10^{15}$ – $10^{16}$  cm<sup>-3</sup>.<sup>[39–44]</sup>

Typical perovskites are cubic or octahedral crystalline structures<sup>[45]</sup> with the ABX<sub>3</sub> chemical formula, where A is a central organic cation (e.g., CH<sub>3</sub>NH<sub>3</sub><sup>+</sup>, [(NH<sub>2</sub>)<sub>2</sub>CH]<sup>+</sup>), or inorganic (e.g., Cs<sup>+</sup>), or mixed cations. B is a divalent metal cation (e.g., Pb<sup>2+</sup>, Sn<sup>2+</sup>, Cu<sup>2+</sup>, Bi<sup>2+</sup>), and X is a halide anion (e.g., Br<sup>-</sup>, I<sup>-</sup>, Cl<sup>-</sup>). Hybrid organic–inorganic perovskites are effective optoelectronic functional materials due to their stable crystal structures and high light absorption. The phase stability of the 3D structure of perovskite (ABX<sub>3</sub>) can be described by the tolerance factor

$$t = \frac{r_A + r_x}{\sqrt{2}(r_B + r_x)} \quad (1)$$

where  $r_A$ ,  $r_B$ , and  $r_x$  are the radii of A, B, and X ions, respectively.<sup>[46]</sup> In general, if the radii of the three ions A, B, and X meet the condition of  $0.9 \leq t \leq 1$ , a stable 3D perovskite structure can be formed.<sup>[46]</sup> Due to the wide variation range of the tolerance factor, the substitution elements of the A, B, and X can be diverse. For the most extensively studied perovskite methylammonium lead iodide (CH<sub>3</sub>NH<sub>3</sub>PbI<sub>3</sub>, also known as MAPbI<sub>3</sub>),  $t = 0.912$ . As is shown in **Figure 2a**, MAPbI<sub>3</sub> is known to exist in the tetragonal ( $\beta$ ) phase at ambient temperature, while adopting the orthorhombic ( $\gamma$ ) structure at lower temperatures (<165 K) and the cubic ( $\alpha$ ) crystal structure at elevated temperatures (>327 K).<sup>[47]</sup>

Theoretical calculations show that Pb plays a critical role in Pb-based perovskites.<sup>[39,40]</sup> Their unique atomic electronic configuration (e.g., Pb 6s lone-pair states, inactive Pb 6p orbital), in combination with high chalcogenide symmetry, strong spin–orbit coupling, and the ionic nature of halides, is recognized to give rise to the high absorption coefficients, long carrier diffusion length and benign defect properties of PSCs.<sup>[39,49]</sup>

**Figure 2b**<sup>[48]</sup> demonstrates that the unoccupied Pb *p* orbitals are dominant in the lower conduction bands (CB) of Pb halide perovskites, whereas the upper valence bands (VB) are mostly I 5*p* orbitals combined with a small fraction of Pb *s* states. The semiconducting properties of MAPbI<sub>3</sub> are primarily derived from the inorganic PbX<sub>6</sub> cage since there are no contributions of C, N, and H atoms (i.e., MA<sup>+</sup>) near the VB maximum and CB minimum.<sup>[50]</sup> The presence of 6s<sup>2</sup> lone-pair electrons of Pb atoms in Pb halide perovskites is the key to their distinguished properties compared with conventional tetrahedral semiconductors used in optoelectronics. The optimal condition for effective optical absorption is the combination of *p*–*p* transitions and a direct band gap. Only compound semiconductors (e.g., PbS, SnS, Sb<sub>2</sub>Se<sub>3</sub>, Bi<sub>2</sub>S<sub>3</sub>), comprising cation elements with lone pair *s* electrons, are capable of *p*–*p* transitions. However, their compounds typically exhibit low symmetry and indirect band gaps. Compared with Si and GaAs, the Pb lone-pair *s* orbitals and material symmetry of Pb halide perovskites give rise to extremely high optical absorption coefficients, which strongly further affects the quantum efficiency of PSCs. In addition, the long carrier diffusion length is strongly correlated with the effective masses (*m*<sup>\*</sup>), nonradiative recombination, and scattering of carriers.<sup>[49]</sup> It is anticipated that the lower CBs of Pb halides and strong *s*–*p* coupling of perovskites would make the upper VB more dispersive than that of conventional *p*–*s* semiconductors. Thus, these properties of Pb atoms contribute to the lengthened carrier diffusion length. Furthermore, Yin et al. also illustrated the unique defect properties of APbX<sub>3</sub>, i.e., the predominant point defects in Pb halide perovskites create only shallow levels and grain boundaries are electrically benign, which is attributed to the antibonding interaction between Pb lone-pair *s* and I *p* orbitals, the strong ionicity, and the large lattice constant (**Figure 2c**).<sup>[49]</sup>

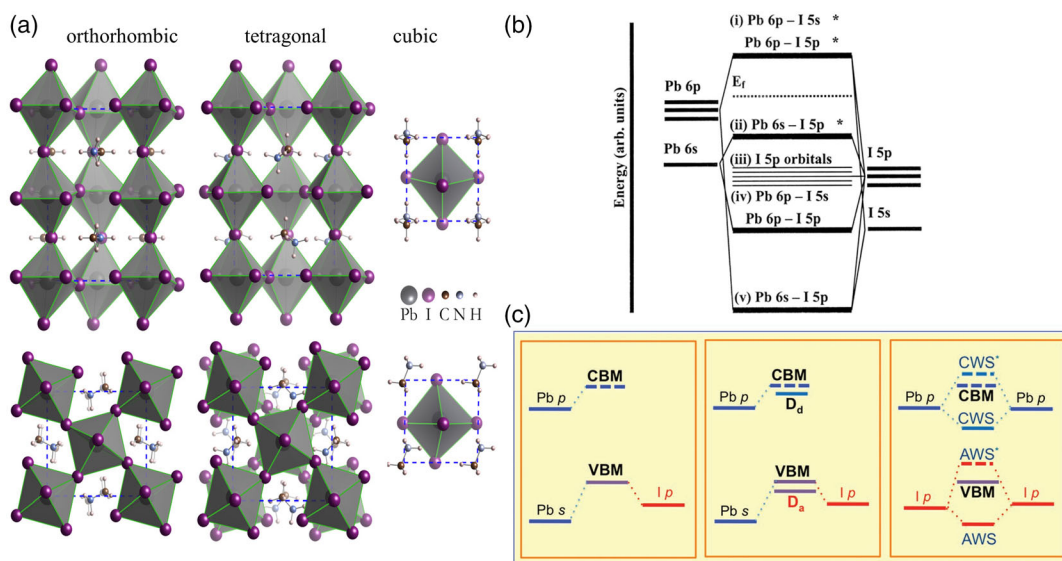


**Figure 2.** a) The crystal structures of the orthorhombic, tetragonal and cubic phases of MAPbI<sub>3</sub>. The upper and lower panels are oriented through 100 and 001, respectively. Reproduced with permission.<sup>[47]</sup> Copyright 2015, American Physical Society. b) Bonding diagram of an isolated [PbI<sub>6</sub>]<sup>4-</sup> cluster. Reproduced with permission.<sup>[48]</sup> Copyright 2003, American Physical Society. c) Schematics of the formation of valence band maximum (VBM) and conduction band minimum (CBM) (left), defects from cation and anion vacancies (middle) and from anion–anion, cation–cation wrong bonds (right). Reproduced with permission.<sup>[49]</sup> Copyright 2015, American Chemical Society.

## 2.2. The Role of Pb in QDSCs

QDs, typically NPs composed of group II–VI or III–V elements, have unique optical properties due to their small particle size ( $\approx 1\text{--}10\text{ nm}$ ), the quantum confinement of electrons and holes, and tunable bandgaps. QDs of the lead salts (PbS, PbSe, and PbTe) exhibited stronger confinement of both electron and hole than well-known II–VI (CdS or CdSe) QDs.<sup>[51]</sup> For example, the electron radius  $\alpha_e$  and hole radius  $\alpha_h$  of PbS are both  $\approx 10\text{ nm}$ , which are much larger than  $\alpha_e \approx 3\text{ nm}$  and  $\alpha_h \approx 1\text{ nm}$  of CdSe. Meanwhile, the highly dispersive optical phonons of the lead salts make the system perfect for researching phonon confinement. In addition, the chemically inactive Pb 6s orbitals are found to play a key role in forming a significantly larger exciton Bohr radius ( $\approx 20\text{ nm}$ ) in QDs than IV–VI and II–VI compounds, which contributes to the highly tunable bandgap, high carrier mobilities, low exciton binding energies, and strong multiple exciton generation (MEG) effects of Pb QDs.<sup>[52]</sup> Similar to PbSe, PbS exhibits high photosensitivity in the near-infrared range, tunable optical bandgap in a range of  $\approx 0.7\text{--}2.1\text{ eV}$ , and multiple exciton production.<sup>[53]</sup>

As a result of these characteristics, PbS QDs have become an especially promising choice for solar cells,<sup>[54,55]</sup> especially when they are combined with perovskites.<sup>[13]</sup> The PbS QD solar cells with a PCE of 13.8% were certified with a monolayer of perovskite bridging the neighboring QDs.<sup>[16]</sup> In addition, a 19.5% (2000 lux indoor light) and an 11.6% efficiency (1.5 Suns concentration) have been demonstrated from ordinary QDSCs (9.55% under 1 Sun).<sup>[17]</sup> Furthermore, by introducing perovskite precursors into the QD solution, Pb chalcogenide QDs can be capped with a perovskite shell, leading to the enhanced stability and performance of solution-processed solar cells.<sup>[56]</sup>

## 3. Causes of Pb leakage from emerging Pb-Based PVs

### 3.1. Causes of Pb Leakage from PSCs

It seems that the Pb leakage is a complicated process resulting from multiple external and internal factors, including the surrounding environmental parameters, perovskite film quality, and perovskite types.<sup>[35]</sup> In this section, we summarize the key parameters that might have a significant impact on the  $\text{Pb}^{2+}$  leaching behavior of PSCs (Figure 3).

#### 3.1.1. External Environmental Triggers for Device Degradation

The characteristics of the perovskite crystal structure are the primary cause of the remarkable PCEs that PSCs have demonstrated to date, as well as the leading causes of its degradation and toxicity issues. Pb-based PSCs may quickly degrade when exposed to water, ultraviolet light, oxygen, heat, or a combination of these factors due to various degrading mechanisms, including polymorphic transformation, hydration, ion diffusion, decomposition, and oxidation.<sup>[57]</sup> It is reported that the stability of the perovskite crystal structure, especially the moisture stability, plays a major role in the initial  $\text{Pb}^{2+}$  leaching rate of PSCs.<sup>[35,58]</sup> Due to the weak ionic bonding in 3D perovskites,

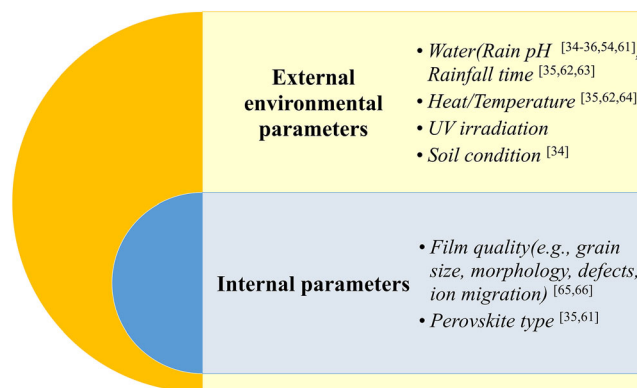
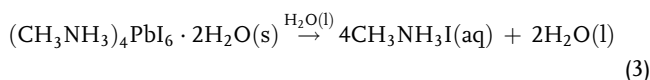
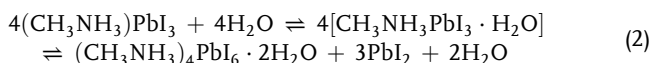


**Figure 3.** The summarized external and internal factors for  $\text{Pb}^{2+}$  leaching from perovskite solar cells (PSCs).

drastic crystal structure decomposition occurs upon long-term exposure to water (in high humidity, rain, dew, or hail).<sup>[59–61]</sup> Yang et al. demonstrated that the decomposition rate was highly dependent on the relative humidity (RH), with high RH (80% to 100%) leading to total degradation in 6 h and low RH (20%) leading to only minor decomposition after several days.<sup>[59]</sup> The specific hydrolysis reaction of perovskite is as follows<sup>[60]</sup>



When exposed to water vapor, monohydrate and dihydrate are formed, which can be converted back to perovskite phases after being soaked in nitrogen. However, liquid water induced  $\text{Pb}^{2+}$  leakage from PSCs is irreversible.<sup>[60]</sup> Due to the crystal structure's susceptibility to water, stability against humidity was examined intensively before its actual commercialization since water is the weakest point of perovskite crystals. The next concern is the light intensity with UV and damp heat, which also accelerates the degradation of PSCs.<sup>[62,63]</sup> The causes of PSC decomposition mentioned earlier are complex and mixed. Nevertheless, these studies indicated that  $\text{PbI}_2$  is the main Pb-containing by-product of the decomposition of  $\text{CH}_3\text{NH}_3\text{PbI}_3$  materials (Figure 4a–c).<sup>[59,62,63]</sup>

#### 3.1.2. Effect of External Weather Conditions for Pb Leakage

As mentioned in the previous section, PSCs are vulnerable to decomposition, under various environmental conditions, which may accelerate  $\text{Pb}^{2+}$  leakage and environmental pollution. The damaged perovskite solar modules can experience different weather conditions, including rain pH, rainfall time, temperature, and soil condition, which are proved to affect the  $\text{Pb}^{2+}$  leakage from PSCs.

**Rain pH:** The pH of rainwater can vary considerably, typically ranging from 4.0 to 9.0.<sup>[64]</sup> Hailegnaw et al. reported 71.9% and 67.5% weight loss of  $\text{Pb}^{2+}$  in  $\text{CH}_3\text{NH}_3\text{PbI}_3$  under acidic rain with pH of 4.2 and 6.0, respectively, and 69.0% weight loss of  $\text{Pb}^{2+}$  under alkaline (pH 8.1) rain.<sup>[58]</sup> Yu et al. studied the leakage

of  $\text{Pb}^{2+}$  from  $\text{MAPbI}_3$ ,  $\text{FA}_{0.85}\text{MA}_{0.15}\text{Pb}(\text{I}_{0.85}\text{Br}_{0.15})_3$ , and  $\text{Cs}_x(\text{MA}_{0.17}\text{FA}_{0.83})_{(100-x)}\text{Pb}(\text{I}_{0.83}\text{Br}_{0.17})_3$  PSCs under simulated rainwater,<sup>[65]</sup> and found that the concentrations of  $\text{Pb}^{2+}$  increased greatly in the early stage at lower pH of 4.5, but the total amount of leached  $\text{Pb}^{2+}$  is within the same order of magnitude under rainwater pH of 5.6 and 4.5 (Figure 5a,b). Su et al. found that the  $\text{Pb}^{2+}$  leaching concentrations in PSCs by different leaching methods of synthetic precipitation leaching procedure test (pH 3.2), toxicity characteristic leaching procedure (TCLP) test (pH 4.93), and water extraction test (WLT) test (pH 7) with a solid-to-liquid ratio of 1:10 were 5.5, 4.8 and 3.0  $\text{mg L}^{-1}$ , respectively.<sup>[36]</sup> Zhai et al. reported that the released  $\text{Pb}^{2+}$  from dissolved  $\text{MAPbI}_3$  (1  $\text{mg L}^{-1}$ ) decreased from 0.369 to 0.318  $\text{mg L}^{-1}$  with increasing pH values from 5.0 to 8.5 after 5 h of leaching.<sup>[34]</sup> Yan et al. reported that the percentage of  $\text{Pb}^{2+}$  leached from  $\text{MAPbI}_3$  increased from  $\approx 53\%$  to 78% when rain water pH decreased from 5 to 1.<sup>[35]</sup> These results suggest that acidic rain can dissolve the  $\text{Pb}^{2+}$  more rapidly, resulting in a higher  $\text{Pb}^{2+}$  leaching rate from PSCs.

**Rainfall Exposure Time:** Several studies have focused on the effect of rainfall exposure time on  $\text{Pb}^{2+}$  leaching from PSCs. Yan et al. performed a kinetic study of the leaching of  $\text{Pb}^{2+}$  of unencapsulated  $\text{MAPbI}_3$ , FAMA-, FAMACs-,  $\text{CsPbI}_3$ -, and  $\text{CsPbI}_2\text{Br}$ -based PSCs under simulated rainfall with a varied spraying time of 10–960 s.<sup>[35]</sup> It is found that  $\text{MAPbI}_3$ -,  $\text{CsPbI}_3$ -, and  $\text{CsPbI}_2\text{Br}$ -based PSCs leached  $\approx 10\%$  of the total amount of  $\text{Pb}^{2+}$  after 10 s of soaking, further increased to  $\approx 60\%$  after 120 s of soaking,  $\approx 90\%$  of the total  $\text{Pb}^{2+}$  leached out after 960 s of leaching.<sup>[35]</sup> Wan et al. studied the  $\text{Pb}^{2+}$  leaching dynamics of cracked  $\text{MAPbI}_3$  (0.5 mL perovskite solution of 1  $\text{mol L}^{-1}$  added to 50 mL rain water) at 45 °C and pH of 5.6.<sup>[66]</sup> Within the first 10 min, Pb dissolving speed decreases from 0.958  $\mu\text{g (L min)}^{-1}$  to 0.135  $\mu\text{g (L min)}^{-1}$ , while Pb dissolving speed is decreased from 0.08 to 0.026  $\mu\text{g (L min)}^{-1}$  when leaching time is increased from 53 to 138 min (Figure 5c), but the  $\text{Pb}^{2+}$  concentration in rainwater keeps increasing.<sup>[66]</sup> Jiang et al. performed contentious leaching of  $\text{Pb}^{2+}$  from  $\text{Cs}_{0.07}\text{FA}_{0.93}\text{PbI}_3$  under constant rainfall for 72 h,<sup>[67]</sup> and found

that the amount of  $\text{Pb}^{2+}$  leakage is increased from 400 to 520 ( $\text{mg m}^{-2}$ ) when the duration of rainfall is increased from 12 to 72 h.

**Temperature:** PSCs can be exposed to a broad temperature range when deployed in different conditions. Wan et al. evaluated the  $\text{Pb}^{2+}$  leakage from encapsulated  $\text{MAPbI}_3$  modules under simulated rainfall (pH = 5.6) with temperatures of 0–85 °C.<sup>[66]</sup> The  $\text{Pb}^{2+}$  leaching rate at 85 °C rapidly rises to 0.029%, which is 11.4 times the leaching rate at 0 °C, and 7.9 times higher than the leaching rate at 45 °C (Figure 5c,d). Yan et al. found that the percentage of  $\text{Pb}^{2+}$  leached from  $\text{MAPbI}_3$  increased from  $\approx 34\%$  to 52% when the temperature is increased from 10–40 °C under 60 s of rainfall exposure.<sup>[35]</sup> Jena et al. studied the degradation of  $\text{MAPbI}_3$  cells at a temperature of 60–120 °C under a humid environment (RH 30–50%).<sup>[68]</sup> The results suggested that elevated temperatures might cause a more rapid decomposition of PSCs, further resulting in a higher  $\text{Pb}^{2+}$  leaching rate of PSCs.

**Soil Condition:** When the leached  $\text{Pb}^{2+}$  is transported into the soil, the soil condition would also affect the  $\text{Pb}^{2+}$  toxicity. Zhai et al. investigated the leaching behavior of  $\text{CH}_3\text{NH}_3\text{PbI}_3$  perovskite NPs in the soil bacterial community under simulated environmental conditions across a range of humic acid (HA) and divalent cation concentrations.<sup>[34]</sup> After 5 h of leaching, an increase of the HA concentration from 0 to 50  $\text{mg L}^{-1}$  induced an increase in the concentration of  $\text{CH}_3\text{NH}_3\text{PbI}_3$  in suspension from 0.445 to 0.537  $\text{mg L}^{-1}$ , but the decrease of concentration  $\text{Pb}^{2+}$  from 0.340 to 0.241  $\text{mg L}^{-1}$  (Figure 5e).<sup>[34]</sup> This indicates that the leakage of free  $\text{Pb}^{2+}$  from  $\text{CH}_3\text{NH}_3\text{PbI}_3$  perovskite in water was mitigated with increasing HA concentration, as surface adsorption of HA blocked the reactive sites of  $\text{CH}_3\text{NH}_3\text{PbI}_3$  perovskite and the formation of HA–metal complexes reduced the amount of free  $\text{Pb}^{2+}$  ions.<sup>[34]</sup> In addition, the increase of divalent cation ( $\text{Ca}^{2+}$  or  $\text{Mg}^{2+}$ ) concentration from 0 to 10 mM induced a decrease of  $\text{CH}_3\text{NH}_3\text{PbI}_3$  perovskite and  $\text{Pb}^{2+}$  concentrations, measured from 0.445 and 0.340  $\text{mg L}^{-1}$  to 0.248 and 0.241  $\text{mg L}^{-1}$  (Figure 5f), respectively, as divalent cations neutralized the surface charge of  $\text{CH}_3\text{NH}_3\text{PbI}_3$ , and reduced its dispersion, which also reduced  $\text{Pb}^{2+}$  release.<sup>[34]</sup>

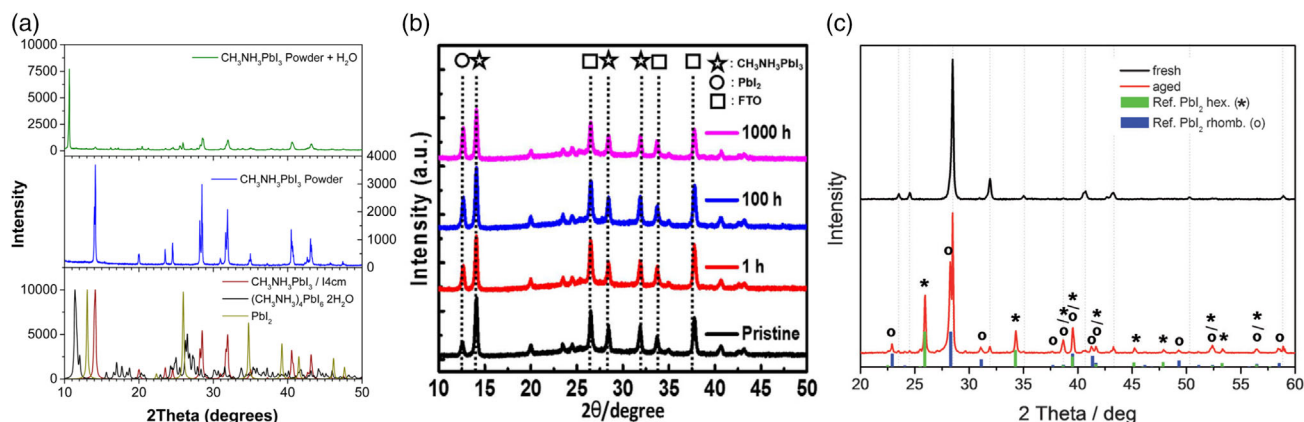


**Figure 4.** X-ray diffraction patterns of: a)  $\text{CH}_3\text{NH}_3\text{PbI}_3$  before (blue) and after (green) the addition of liquid water, and the calculated patterns. Reproduced with permission.<sup>[59]</sup> Copyright 2015, American Chemical Society. b) The devices upon UV exposure. Reproduced with permission.<sup>[62]</sup> Copyright 2016, Springer Nature. c) A fresh and an aged (for 72 h) sample exhibiting the production of  $\text{PbI}_2$  as due to decomposition. Reproduced with permission.<sup>[63]</sup> Copyright 2015, Wiley-VCH GmbH.

### 3.1.3. Internal Causes of Pb Leakage

**Effect of Film Quality on Pb Leakage:**  $Pb^{2+}$  leakage is potentially related to the quality of perovskite materials (e.g., grain size, morphology, the concentration of defects, and type of exposed surface). The nucleation of perovskite films is often accompanied by the formation of many defects. The crystal defects can be a vacancy in the crystal elements ( $A^+$ ,  $Pb^{2+}$ , or  $X^-$ ) or contamination within or on the surface of the crystal grain. It has been reported that defects at grain boundaries and interfaces might serve as charge accumulation sites and infiltration pathways and trigger irreversible degradation of the perovskite film.<sup>[69,70]</sup> In addition, due to the ionic nature of perovskite materials, defects may accumulate in bulk perovskite/interface perovskite crystal materials (e.g., ion migration), which may also play a significant role in  $Pb^{2+}$  leakage.

**Effect of Perovskite Type on Pb Leakage:** So far, there are only a few reports that investigate  $Pb^{2+}$  leakage in different types of PSCs. Recent studies reported that the  $Pb^{2+}$  leaching rate strongly depends on the type of PSCs, pointing to a potential route toward  $Pb^{2+}$  leaching reduction through materials optimization.<sup>[35,65]</sup> Yan et al. reported the kinetic behavior of  $Pb^{2+}$  leaching from five types of PSCs under static soaking and rainfall conditions. After 10 days static soaking, the total  $Pb^{2+}$  leaching amount of MAPbI<sub>3</sub>-, FAMA-, FAMACs-, CsPbI<sub>3</sub>-, and CsPbI<sub>2</sub>Br-based PSCs was 438.26, 917.50, 943.45, 439.77, and 493.54 mg m<sup>-2</sup>, respectively (Figure 6a).<sup>[35]</sup> The results

suggested that absolute Pb quantity in perovskite films affects the total amount of  $Pb^{2+}$  leached out into the water. The percentage of leached  $Pb^{2+}$  of total Pb amount in CsPbI<sub>2</sub>Br-based PSC was highest (97.3%), compared to 91.2%, 91.8%, 60.4% and 84.9% for MAPbI<sub>3</sub>-, FAMA-, FAMACs- and CsPbI<sub>3</sub>-based PSCs, respectively, after 960 s of rainfall exposure (Figure 6b).<sup>[35]</sup> Under rainfall exposure conditions of 120–960 s, CsPbI<sub>2</sub>Br- and FAMACs-based PSCs show the highest and lowest  $Pb^{2+}$  leachability, respectively.<sup>[35]</sup> Yu et al. demonstrated a two-stage dissolution process (dissolution of ammonium halides and lead halides) of  $Pb^{2+}$  ions from three different types of PSCs (MAPbI<sub>3</sub>, FA<sub>0.85</sub>MA<sub>0.15</sub>Pb(I<sub>0.85</sub>Br<sub>0.15</sub>)<sub>3</sub> and Cs<sub>x</sub>(MA<sub>0.17</sub>FA<sub>0.83</sub>)<sub>(100-x)</sub>Pb(I<sub>0.83</sub>Br<sub>0.17</sub>)<sub>3</sub>), and found that the amount of  $Pb^{2+}$  leaching is within the same order of magnitude among the three types of perovskite films after 1 day soaking.<sup>[65]</sup>

### 3.2. Causes of Pb Leakage from QDSCS

Many factors affect the toxicity of QDs, including the physicochemical properties of the particles themselves (e.g., particle size, stability, dispersion, surface charge, surface modification groups, oxygenation state), the concentration of QDs, type of recipient cells (in vivo), and incubation time.<sup>[18,71–73]</sup> Therefore, the toxicity of QDs should not be simply defined, but should be based on a comprehensive analysis of the intrinsic properties of the dots and their interaction with the external environment. Chen et al. elucidate the origin of the structure degradation as well as the device

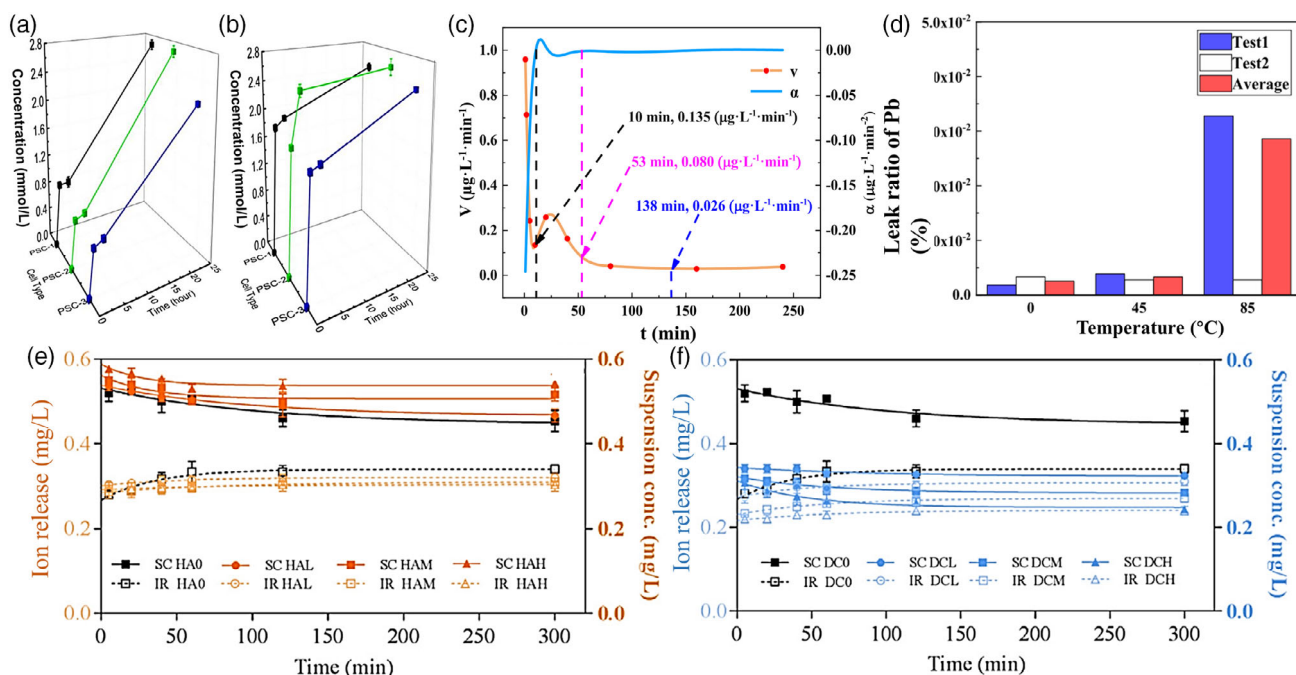


**Figure 5.** a)  $Pb^{2+}$  contents in the contaminated rainwater of MAPbI<sub>3</sub> (PSC-1), FA<sub>0.85</sub>MA<sub>0.15</sub>Pb(I<sub>0.85</sub>Br<sub>0.15</sub>)<sub>3</sub> (PSC-2), and Cs<sub>x</sub>(MA<sub>0.17</sub>FA<sub>0.83</sub>)<sub>(100-x)</sub>Pb(I<sub>0.83</sub>Br<sub>0.17</sub>)<sub>3</sub> (PSC-3), at pH = 5.6 and b) pH = 4.5 depending on leaching time. Reproduced with permission.<sup>[65]</sup> Copyright 2016, American Chemical Society; c) The Pb dissolving speed ( $v$ ) and the derivative of dissolving speed ( $\alpha$ ) of MAPbI<sub>3</sub> modules under conditions of 45 °C and pH = 5.6. Reproduced with permission.<sup>[66]</sup> Copyright 2021, Elsevier; d)  $Pb^{2+}$  leaking ratio at different temperatures when MAPbI<sub>3</sub> modules were soaked into 100 mL simulated rainwater (pH = 5.6). Reproduced with permission.<sup>[66]</sup> Copyright 2021, Elsevier; e) Dissolution kinetics of CHNH<sub>3</sub>PbI<sub>3</sub> under different environmental conditions of HA and f) divalent cations (DC), IR: Pb ion release. DCL: divalent cations 1 mM, DCM: divalent cations 2.5 mM, DCH: divalent cations 10 mM; HAL: HA 10 mg L<sup>-1</sup>, HAM: HA 25 mg L<sup>-1</sup>, HAH: HA 50 mg L<sup>-1</sup>. Reproduced with permission.<sup>[32]</sup> Copyright 2020, Elsevier.

performance degradation of PbS QDSCs with an operando measurement which ruled out environmental parameters such as moisture, oxygen, and temperature. The grazing-incidence small-angle X-ray scattering and grazing-incidence wide-angle X-ray scattering measurements revealed the initial structure degradation of PbS QDSCs, and indicated that the “light-soaking” effect decreased interdot spacing of QDs in the active layer while increasing the spatial disorder. In addition, the overall lattice compression was confirmed during the burn-in degradation process. This work suggested that the device’s stability could be achieved by the positional stabilization of the QDs inside the QD solid, which might result in reduced  $Pb^{2+}$  leaching.<sup>[71]</sup>

## 4. Ecotoxicity of emerging Pb-Based PVs

### 4.1. Environmental Impact of Pb from PSCs

#### 4.1.1. Effect of $Pb^{2+}$ Leakage from PSCs on Water, Soil, and Air

To understand the potential environmental impact of PSCs, a number of studies have been conducted to investigate the leakage of  $Pb^{2+}$  from PSCs.<sup>[26,27,30–32,34]</sup> When suffering from water and fire exposure,  $Pb^{2+}$  can easily release from PSCs and migrate through water, soil, and air (Figure 7), causing severe impacts on the ecosystem and human health.<sup>[26,27,34,35]</sup>

A growing research effort has been dedicated to understanding the  $Pb^{2+}$  leakage from PSCs in the presence of moisture and liquid water.<sup>[35,36,58,65–67,74]</sup> Su et al. evaluated the leaching concentration of  $Pb^{2+}$  from PSCs and found that the amount of  $Pb^{2+}$  exceeded the hazardous waste limit of  $5\text{ mg L}^{-1}$ ,<sup>[36]</sup> and  $Pb^{2+}$  was found to continuously leach out in the leaching cycles of water extraction. Hailegnaw et al. reported 72% loss of Pb from  $CH_3NH_3PbI_3$  perovskite films after 5 min exposure to simulated rain water (pH 4.2),<sup>[58]</sup> and the leached Pb species include both soluble  $Pb^{2+}$  and  $PbI_2$  solid or colloids. Yu et al. studied the  $Pb^{2+}$  leaching from  $MAPbI_3$ ,  $FA_{0.85}MA_{0.15}Pb(I_{0.85}Br_{0.15})_3$  and  $Cs_x(MA_{0.17}FA_{0.83})_{(100-x)}Pb(I_{0.83}Br_{0.17})_3$  PSCs under simulated normal (pH = 5.6) and acidic (pH = 4.5) rainwater.<sup>[65]</sup> The concentration of  $Pb^{2+}$  first increased to 0.7 and  $\approx 1.7\text{ mmol L}^{-1}$  in normal rain and acidic rain, respectively, and all gradually reached  $2\text{--}2.7\text{ mmol L}^{-1}$  after 1 day of leaching.<sup>[65]</sup> Panthi

et al. examined that the concentration of leached  $Pb^{2+}$  in  $MAPbI_3$  was as high as  $6.6\text{ mg L}^{-1}$  through the toxic characteristic leaching method (pH 4.93).<sup>[74]</sup> Wan et al. observed that Pb leaching ratios of encapsulated and unencapsulated  $MAPbI_3$  modules were 2.41% and 100%, respectively, when broken PMs were washed by acid rainwater (pH = 5.6) at  $85\text{ }^\circ\text{C}$  for more than 4 h.<sup>[35,66]</sup> Jiang et al. reported that Pb in  $Cs_{0.07}FA_{0.93}PbI_3$  films leached out entirely at  $0.54\text{ g m}^{-2}$  from damaged PSCs when exposed to simulated heavy rain for 72 h.<sup>[67]</sup> It is thus clear that  $Pb^{2+}$  could easily leak out of PSCs in the case of physical damage, failure of encapsulation, or exposure to liquid water.

The solubility of the Pb species leached from PSCs is often associated with high environmental mobility, indicating an increased risk of soil contamination due to  $Pb^{2+}$  leaching from perovskite. Haliegnaw et al. estimated that the  $Pb^{2+}$  concentration of the soil surface layer ( $\approx 1\text{ cm}$  thick) below the  $CH_3NH_3PbI_3$  perovskite solar panels would increase to  $\approx 70\text{ ppm}$ .<sup>[58]</sup> Moody et al. reported that the  $Pb^{2+}$  contamination levels for air, soil, and surface water are  $0.2\text{ }\mu\text{g m}^{-3}$ ,  $100\text{ mg kg}^{-1}$ , and  $15\text{ }\mu\text{g mL}^{-1}$ , respectively, resulting from the landfilling of a hypothetical 5 mega-watt-peak ( $MW_p$ ) perovskite solar plant.<sup>[24]</sup> Schmidt et al. found that the dissolution half-lives of Pb in  $MAPbI_3$  and  $CsFAPbI_3$  were all below 1 h (maximum of  $t_{50\%} = 0.86\text{ h}$  for MAPI under anaerobic conditions) with  $100\text{ mg Pb kg}^{-1}$  soil and a soil/water ratio of 1/5 ( $\text{m}^{-1}$ ), and 92–98% of  $Pb^{2+}$  was removed into aqueous phase after 24 h.<sup>[75]</sup> Although only 3.7–8.1% of  $Pb^{2+}$  leached from PSCs would affect the soil biota after entering the soil,  $Fe^{3+}$ ,  $Mn^{4+}$  oxides or soil acidification may result in partial re-mobilization of the  $Pb^{2+}$ .<sup>[56]</sup>

Besides water and soil,  $Pb^{2+}$  can escape from PSC into the air during a fire. Conings et al. experimentally investigated the release of  $Pb^{2+}$  from  $Rb_{0.05}(Cs_{0.05}(FA_{0.83}MA_{0.17})_{0.95})_{0.95}Pb(I_{0.90}Br_{0.10})_3$  at  $760\text{ }^\circ\text{C}$  in a tube furnace, and found that perovskite without a glass cover decomposed into  $PbI_2$  at high temperatures, and then transformed into  $PbO/PbO_2$  due to evaporation and oxidation.<sup>[76]</sup> Yoo et al. demonstrated that PSCs degraded into  $PbI_2$  and  $PbO$  after hydrolysis and combustion in case of fire.<sup>[77]</sup> Babayigit et al. estimated that PSCs would release a maximal 20 g of Pb per roof in a simulated sudden fire scenario, assuming an average roof size of  $100\text{ m}^2$  with 50% PSC coverage.<sup>[20]</sup> In summary,  $Pb^{2+}$  in PSCs would be emitted into water, soil,

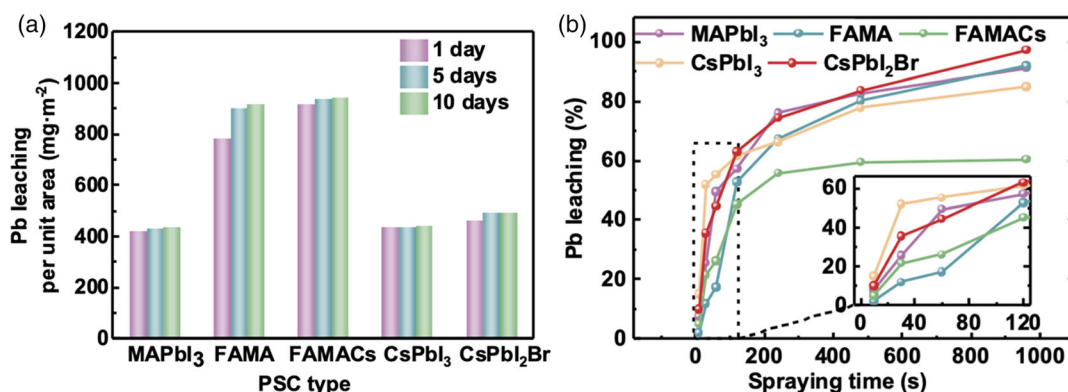


**Figure 6.**  $Pb^{2+}$  leaching dynamics of the five types of PSCs. a)  $Pb^{2+}$  leaching per unit area from 1–5 days under static soaking. b)  $Pb$  leaching percentage at 0–960 s intervals under pure water rainfall exposure, insert is 0–120 s intervals. Reproduced with permission.<sup>[35]</sup> Copyright 2021, Elsevier.

and air environment in the forms of lead iodide (PbI<sub>2</sub>), lead oxide (PbO/PbO<sub>2</sub>), and ionic metals (Pb<sup>2+</sup>, Si<sup>2+</sup>, Al<sup>3+</sup>), posing risks of Pb<sup>2+</sup> contamination of the ecosystem due to its high transability.

#### 4.1.2. Effect of Pb Leakage from PSCs on Biological Systems

Since the Pb<sup>2+</sup> leached from PSCs can be readily adsorbed in soil, soil plants and bacteria have been investigated to evaluate the effect of PSCs on soil ecotoxicology. For mints plants (*Mentha spicata*) grown in the uncontaminated soil, the Pb concentrations were 9.3–15.2, 2.8–3.9, and 7.5–8.4 mg kg<sup>-1</sup> for roots, stems, and leaves, respectively, whereas the Pb<sup>2+</sup> content in mint grown in MAPbI<sub>3</sub> and PbI<sub>2</sub> contaminated soil significantly increased to 3401.1–4896.8, 179–240.1, and 384.7–426.8 mg kg<sup>-1</sup> for roots, stems, and leaves, respectively.<sup>[26]</sup> These values are far higher than the safety values of the agricultural industry in China, indicating a bioaccumulation potential of Pb in food chains. Wang et al. conducted a battery of in vivo toxicity for three Pb-based PSCs (CH<sub>3</sub>NH<sub>3</sub>PbI<sub>3</sub>, NH<sub>4</sub>CH<sub>3</sub>NH<sub>3</sub>PbBr<sub>3</sub>, and CH<sub>3</sub>NH<sub>3</sub>PbBr<sub>3</sub>) among *Vibrio fischeri*, *Pseudomonas putida*, and natural microbes extracted from soils, as shown in **Figure 8**.<sup>[27]</sup> CH<sub>3</sub>NH<sub>3</sub>PbBr<sub>3</sub> was identified as the most toxic Pb-based PSCs to soil microbes with an effective concentration of 50% (EC50) value of 8.07 (6.65–9.85) mg L<sup>-1</sup>, followed by CH<sub>3</sub>NH<sub>3</sub>PbI<sub>3</sub> with an EC50 value of 9.27 (7.96–10.76) mg L<sup>-1</sup>, and NH<sub>4</sub>CH<sub>3</sub>NH<sub>3</sub>PbBr<sub>3</sub> with an EC50 value of 12.81 (10.64–15.34) mg L<sup>-1</sup>. *V. fischeri* showed the highest sensitivity with EC50 values (30 min exposure) ranging from 1.45 to 2.91 mg L<sup>-1</sup>.

Recent studies have focused on the biological impacts of PSCs on organisms in aquatic environments, including, fishes,<sup>[28–31]</sup> water fleas,<sup>[28]</sup> phytoplankton,<sup>[33]</sup> Chironomus,<sup>[29]</sup> and nematodes.<sup>[27–29]</sup> Kwak et al. found that Pb was the most leachable component in the leachates of broken perovskite MAPbI<sub>3</sub> solar cells, with a concentration of 0.28–4.37 mg L<sup>-1</sup>. The EC50 values were 25.75% for fish embryos at 7 days post fertilization, and >50% for water fleas.<sup>[28]</sup> Kwak et al. found that PbI<sub>2</sub>-treated zebrafish and Japanese medaka exhibited multiple adverse effects (e.g., growth reduction, tail malformation, spine deformity, hemostasis, and edema deformation in organs) with increasing PbI<sub>2</sub> exposure concentration from 1 to 20 mg L<sup>-1</sup>.<sup>[29]</sup> Bae et al. compared the toxicity of perovskite MAPbI<sub>3</sub> to four ecotoxicity species, where the order of their ecotoxicity was *D. magna*>*D. rerio*>*C. elegans*>*C. riparius*.<sup>[30]</sup> Based on *C. elegans* in 72 h reproduction, the mean EC50 values were 0.59, 5.05, 2.65, and 4.30 mg L<sup>-1</sup> for Pb<sup>2+</sup>, PbI<sub>2</sub>, PbO, and PSC, respectively. Liu et al. reported that *S. obliquus* growth was remarkably inhibited when the initial MAPbI<sub>3</sub> perovskite level (CPL) was above 40 mg L<sup>-1</sup>.<sup>[33]</sup> And when the CPL was over 5 mg L<sup>-1</sup>, the survival of *D. magna* was notably threatened. The 72 h EC50 of *S. obliquus* was calculated as 37.21 mg L<sup>-1</sup>, and the 24 h LC50 to *D. magna* adults and neonates were calculated as 37.53 and 18.55 mg L<sup>-1</sup>, respectively. The aforementioned research suggests that leachable Pb from PSCs induces high toxicity to aquatic organisms even at low concentrations.

#### 4.1.3. Effect of Pb Leakage from PSCs on Human Health

As Pb is not biodegradable, it will finally accumulate in the human body within the food chain. Chronic Pb poisoning would

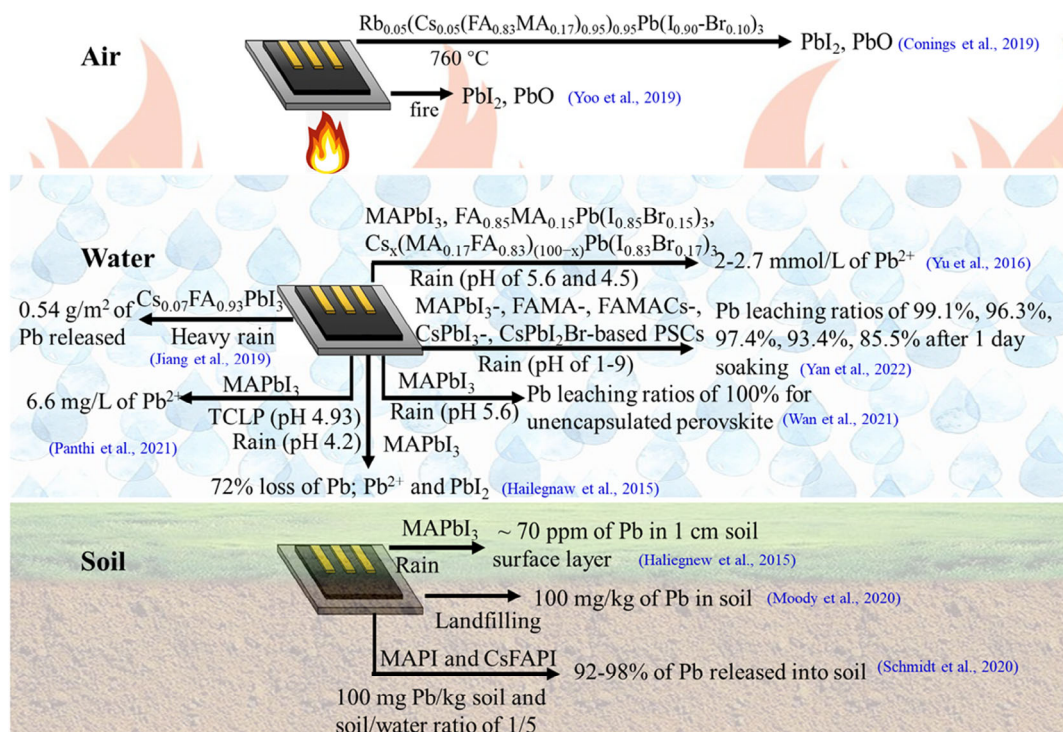


**Figure 7.** Illustration of research conducted to evaluate the leakage of PSC materials under different weather conditions.

occur when the Pb level in the blood reaches  $5 \mu\text{g dL}^{-1}$ ,<sup>[78]</sup> owing to the transport of Pb in the human body via the blood circulation system through mimicry of essential elements of  $\text{Ca}^{2+}$ ,  $\text{Fe}^{2+}$ , and  $\text{Zn}^{2+}$ .<sup>[79]</sup> Most Pb in the human body distributes in soft tissue and skeletal systems. In soft tissues, Pb can interfere with cells of living organisms, including liver, kidneys, central nervous, and reproductive systems and cause severe damage to human health, such as hypertension, anemia, impaired nerve conduction, encephalopathy, and even death.<sup>[79,80]</sup> Continuous exposure to Pb would induce gradual fixation to bones as insoluble Pb phosphate, which requires 40–50 years of decomposition. Much worse, Pb is evacuated through breast milk and placenta. This represents a major risk for breastfed infants and fetuses, who are more susceptible to heavy metal intoxication.<sup>[79]</sup>

Excessive levels of Pb from PSCs have been detected in vegetables and animals.<sup>[26–31,33]</sup> As a consequence, these poisonous Pb could be transferred from soil/water and accumulated in human beings through the biological cycle. Thus, the impact of PSCs on human cell lines (A549 cell, SH-SY5Y cell, Caco-2/TC7 cell, Beas2B cell, and HepG2 cell) and mouse neurons were assessed via in vitro assay.<sup>[26–31,33]</sup> Benmessaoud et al. reported the effects of perovskite  $\text{MAPbI}_3$  on human lung adenocarcinoma epithelial cells (A549) (Figure 9a) and human dopaminergic neuroblastoma cells (SH-SY5Y) (Figure 9b).<sup>[32]</sup> When hippocampal primary neurons and neuroblastoma cells were exposed to dissolved  $\text{MAPbI}_3$ , they suffered a massive apoptotic cell death, whereas A549 cells experienced significantly altered proliferation kinetics, cellular morphology, and metabolic activity without noticeable cell death. The toxic effect of  $\text{MAPbI}_3$  was attributed to the  $\text{Pb}^{2+}$  and MA ions. Wang et al. conducted in vivo toxicity tests for three Pb-based PSCs ( $\text{CH}_3\text{NH}_3\text{PbI}_3$ ,  $\text{CH}_3\text{NH}_3\text{PbBr}_3$ , and  $\text{CH}_3\text{NH}_3\text{PbI}_2\text{Br}$ ) using human cell models (A549) and human colonic epithelial CaCo-2 subclone TC7 cells (Caco-2/TC7).<sup>[27]</sup> The results confirmed that the  $\text{CH}_3\text{NH}_3\text{PbBr}_3$  was the most noxious of the Pb-based PSCs. Pb-based PSCs showed slight cytotoxic activity against A549 cells over the entire concentration range of  $1\text{--}100 \text{ mg L}^{-1}$  (Figure 9c). In contrast,

Pb-based PSCs significantly impeded the growth of Caco-2/TC7 cells, inhibiting 42.79–63.46% of cells compared with the control at an exposure dose of  $100 \text{ mg L}^{-1}$  (Figure 9d).<sup>[27]</sup> Bae et al. evaluated the cytotoxicity of  $\text{MAPbI}_3$  by two human cell lines (Beas2B and HepG2).<sup>[30]</sup> The results show that exposure to  $100 \text{ mg L}^{-1}$  of  $\text{MAPbI}_3$  exposure led to about 20 to 40% cytotoxicity in Beas2B cells. Pb species caused lesser toxicity to HepG2 cells (i.e., 10% to 20%) than to Beas2B cells. Therefore, it can be found that the leakage of Pb-related compounds from PSCs possesses substantial environmental hazards to water, soil, and air. When these P-related products are absorbed by organisms or the human body, it will cause significant toxic effects.

## 4.2. Environmental Impact and Ecotoxicity of Pb-Based QDSCs

### 4.2.1. Environmental Impact of Pb from PbS QDSCs

Yan et al. indicated that Pb leaching from PbS QDSCs is comparable to that of PSCs.<sup>[35]</sup> When soaking in rainwater for 3 days, the leakage amount of lead per unit area for PbS QDSC,  $\text{MAPbI}_3$ , FAMA, FAMACs,  $\text{CsPbI}_3$ , and  $\text{CsPbI}_2\text{Br}$  were about 450, 210, 500, 350, 150, and  $200 \text{ mg m}^{-2}$ , respectively. Moreover, the amount of leached Pb per unit area from PbS QDSCs under 30, 60, and 90 s soaking time were 20.41, 47.96, and  $59.13 \text{ mg m}^{-2}$ , respectively, suggesting a very rapid leaching of Pb from PbS QDSCs.<sup>[35]</sup> Truong et al. measured the concentrations of leached Pb in fresh and 5 days aged PbS-MT and PbS-DT solutions ( $3 \text{ mg mL}^{-1}$ ) after 18 h soaking.<sup>[81]</sup> Pb concentrations of fresh PbS-MT and PbS-DT solutions were 1927 and  $2270 \text{ mg L}^{-1}$ , respectively, whereas, the Pb levels from aged PbS-MT and PbS-DT solutions were 87 and  $1.075 \text{ mg L}^{-1}$ , respectively.<sup>[81]</sup> The results indicated that the PbS-MT and PbS-DT NPs decomposed over time, releasing ionic Pb into the solution. Chang et al. observed Pb dissolution of PbS nanocrystals in bronchial epithelial cell growth medium (BEGM) at  $37^\circ\text{C}$  for 24 h, and the Pb-ion content in the supernatant was  $\approx 4, 6, 9, \text{ and } 11 \text{ mg mL}^{-1}$  for PbS T-octahedron, cuboctahedron,

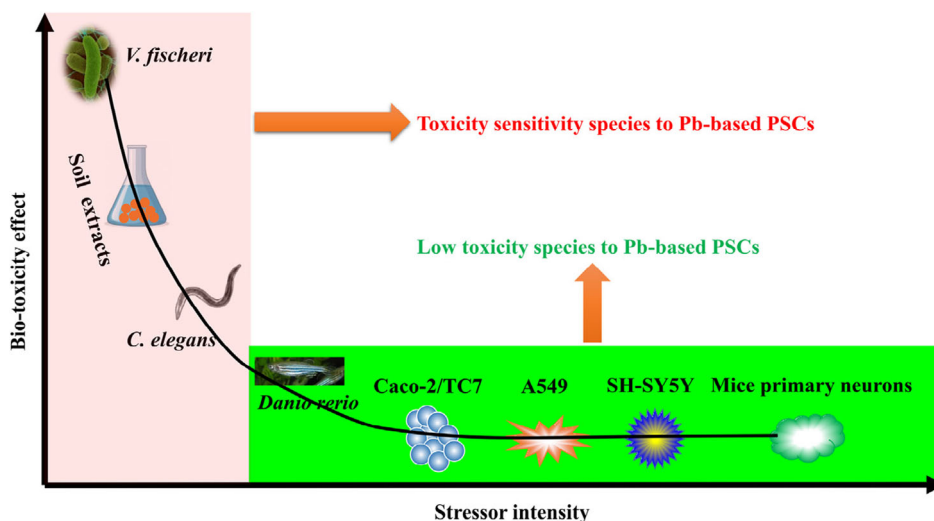


**Figure 8.** Schematic diagram of Pb-based PSCs toxicity sensitivity to tested organisms based on the EC<sub>50</sub> values. The toxicity data of *Danio rerio*, SH-SY5Y, and mice primary neurons were derived from previous literature reports.<sup>[31,32]</sup> Reproduced with permission.<sup>[27]</sup> Copyright 2020, Elsevier.

T-cube, and cube nanocrystals, respectively.<sup>[82]</sup> Moody et al. reported that the concentrations of Pb leached from PbS QDSCs (ITO/ZnO/PbS ink/Au) made with TBAI and PbX<sub>2</sub> ink preparations were 4 and 10.5 mg L<sup>-1</sup>, respectively. The leached Pb level is determined by the toxicity characteristic leaching procedure (TCLP, leached in an acetic acid buffer solution of pH = 4.98 with a liquid/solid ratio of 20/1 ratio and 18 ± 2 h soaking). The results indicated that the leached concentration of Pb from PbS QD made with PbX<sub>2</sub> ink is greater than the regulatory limits specified by the EPA (5 mg L<sup>-1</sup> for Pb), and PbS QD made with PbX<sub>2</sub> ink can be classified as hazardous waste and requires expensive treatment.

#### 4.2.2. Toxicity of Pb from PbS QDSCs

Although there is insufficient research on the toxicity of PbS QDSCs, the ecotoxicity of PbS QDSCs can be inferred from PbS QDs. As the high environmental mobility of Pb, some researchers studied potential health hazards of PbS QDs to mouse cells,<sup>[83]</sup> human cells,<sup>[82,83]</sup> embryonic zebrafish,<sup>[81]</sup> and various organs of rats.<sup>[84,85]</sup> Kim et al. evaluated the biocompatibility of PbS QDs in human (HEK293 and THP-1) and mouse (TCMK-1 and AML12) cells.<sup>[83]</sup> When HEK293 cells exposed to 2, 6, 25, 100, and 400 µg mL<sup>-1</sup> PbS-MPA, cell proliferation

was decreased to 97%, 85%, 63%, 38%, and 38%, respectively (Figure 10a).<sup>[83]</sup> Under 150 µg mL<sup>-1</sup> of PbS-MPA exposure, cell proliferation of human THP-1 and mouse TCMK-1 and AML12 cells to PbS-MPA was decreased to ≈35, ≈20, and ≈90%, respectively (Figure 10b).<sup>[83]</sup> The DNA damage in HEK293 cells occurred for cells exposed to 5 µg mL<sup>-1</sup> PbS-MPA.<sup>[83]</sup> Chang et al. investigated the toxicity behaviors of PbS nanocrystals in BEAS-2B cells.<sup>[82]</sup> Cell viability of BEAS-2B cells decreased from 100 to ≈40% when treated with 0.4 to 200 µg mL<sup>-1</sup> PbS cube nanocrystals for 24 h (Figure 10c). When BEAS-2B cells were treated with 6.25 µg mL<sup>-1</sup> PbS nanocrystals for 24 h, the Pb content/protein can reach ≈0.029 µg µg<sup>-1</sup>.<sup>[82]</sup> They found that the toxicity of PbS nanocrystals was ascribed to the low Pb dissolution of {111} facets because of the strong protection afforded by poly (vinyl pyrrolidone) during synthesis.<sup>[82]</sup> Truong et al. investigated in vivo biological responses of embryonic zebrafish (*Danio rerio*) when exposed to PbS-NPs.<sup>[81]</sup> Per embryo at 12 hpf had the highest (≈100 ng) tissue concentration of Pb when exposed to 160 µg mL<sup>-1</sup> of PbS-MT (Figure 10d). Embryos exposed to 10–320 µg mL<sup>-1</sup> solutions of PbS-MT, DT, and Pb(NO<sub>3</sub>)<sub>2</sub> at 6 hpf and sampled at 12 hpf, had Pb concentration in tissue ranging from ≈0.1 to 100 ng (Figure 10d).<sup>[81]</sup> Embryos exposed to PbS-MT at 320 µg mL<sup>-1</sup> did not survive at the sampling time.<sup>[81]</sup> Cao et al. measured Pb content in various organs of male Sprague Dawley (SD) rats, and confirmed the

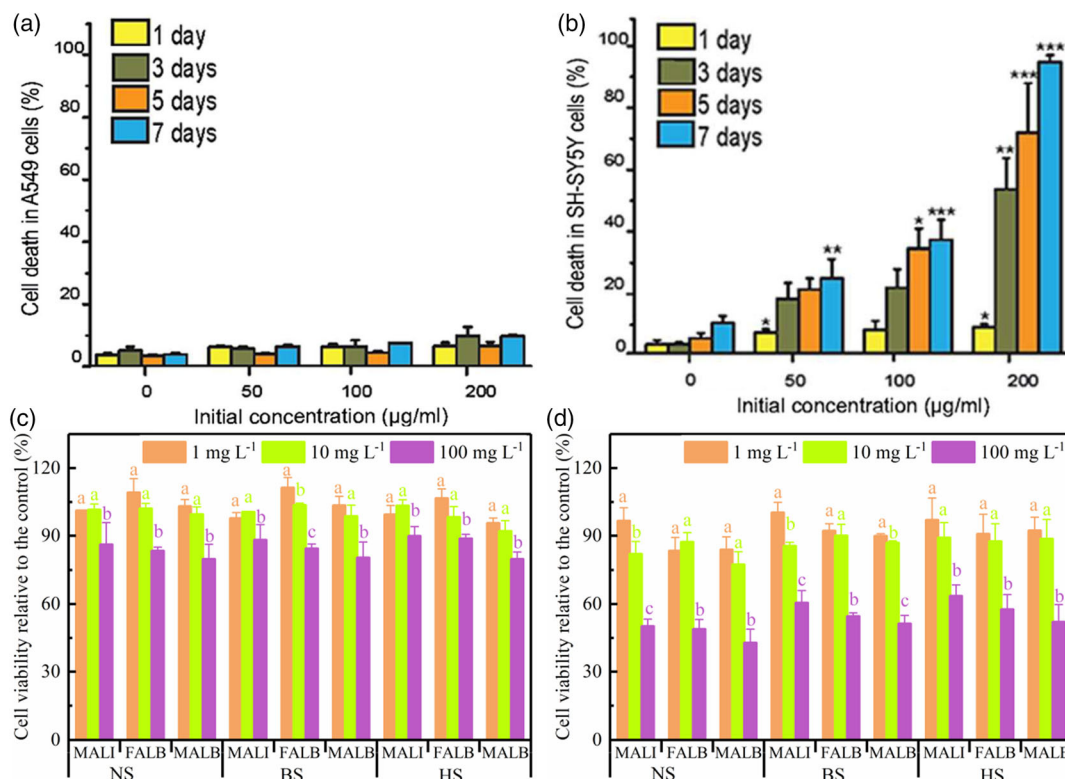


**Figure 9.** a) MAPbI<sub>3</sub> induced cell death of SH-SY5Y neuroblastoma cells and b) A549 human lung epithelial cells. The cell death level is expressed as the percentage of cells with a compromised cell membrane (SG positive cells) to the total cell number. Reproduced with permission.<sup>[32]</sup> Copyright 2020, Royal Society of Chemistry c) Cytotoxic effects of Pb-based PSCs on A549 human alveolar epithelial cells and d) Caco-2/TC7 human colonic epithelial cells. The data represent the percentage cytotoxicity compared with control cells (exposed to cell culture medium). NS, BS, and HS represent the Pb-based PSCs pre-incubated with no serum added, Bovine serum added, and Human serum added for 1 h at 37C, respectively. Reproduced with permission.<sup>[27]</sup> Copyright 2020, Elsevier.

high neurotoxicity of PbS NPs.<sup>[84]</sup> Pb levels in rats' organs of heart, liver, lung, kidney, and bone would reach  $\approx 1.5$ ,  $\approx 45$ ,  $\approx 13$ ,  $\approx 118$ , and  $\approx 120 \mu\text{g g}^{-1}$ , respectively, under high dose treatment ( $30 \text{ mg kg}^{-1}$ ) and exposed to PbS NPs by trachea once every 7 days for 3 consecutive months (Figure 10e).<sup>[84]</sup> Li et al. observed the pathological changes in lung tissue of adult specific-pathogen-free Sprague–Dawley male rats under exposure to PbS NPs.<sup>[85]</sup> After exposure to PbS NPs by injection once a week for 4 months, Pb levels in whole blood and lung tissues of rats were  $1.209$  and  $3.558 \mu\text{g g}^{-1}$  under  $60 \text{ nm}$  PbS NPs treatment, and  $1.642$  and  $5.631 \mu\text{g g}^{-1}$  under  $30 \text{ nm}$  PbS NPs treatment.<sup>[85]</sup> In summary, many researchers confirmed that PbS QDs had high toxicity to animal and human health; thus, the development of effective strategies for Pb leakage reduction is essential.

## 5. Toxicity reduction strategies

### 5.1. Pb toxicity reduction strategies for PSCs

As a layer-stacked device, the optimization of each functional layer and its interlayers is key to the performance of PSCs. Typical PSC structure consists of transparent electrodes (ITO, FTO, etc.), hole transport layer (HTL, i.e., Spiro-OMeTAD, PEDOT: PSS, PTAA), perovskite light-absorbing layer, electron transport layer (ETL, i.e.,  $\text{C}_{60}$ , PCBM), upper metal electrodes (gold, silver, copper, etc.) and modification layers inserted as interlayers.<sup>[86]</sup> To minimize the toxicity, several Pb-containing

methods have been explored in PSCs by further optimizing their material design (e.g., using Pb-less perovskites, additives in PSC functional layers), device architectures (e.g., employing interfacial modifiers), and encapsulation strategies.

#### 5.1.1. Pb-Free or Pb-Less PSCs

The perovskite material can be regulated to various compositions to obtain optimal optoelectronic properties.<sup>[87]</sup> Thus, Pb has been replaced entirely (Pb-free) or partially (Pb-less) in PSCs for  $\text{Pb}^{2+}$  toxicity elimination or reduction.

Pb has been substituted by less-toxic metal elements (such as Sn, Ge, Cu), which can theoretically be applied in PSC devices, while their PCE and stability are still far below the standards for industrial applications.<sup>[40,88–90]</sup> Among them, Sn and Ge are ideal Pb-substituting elements in PSC devices because they have similar ionic half-valences and extranuclear electron distributions to Pb elements.<sup>[91,92]</sup> However, due to the poor chemical stability and solubility of  $\text{Ge}^{2+}$  in polar solvents, Ge-based halide perovskites have achieved only 0.6% PCE so far.<sup>[93]</sup> Sn-based perovskites are the most promising alternatives to Pb-based perovskites because their bandgaps are close to the optimal value for PV applications (1.1 eV), combined with strong light absorption (up to 950 nm) and good carrier mobility.<sup>[94,95]</sup> In recent years, the PCE of Sn-based PSCs has been significantly improved, while the highest PCE of PV devices prepared based on Sn-based perovskite is 14.81% achieved in  $\text{FaSnI}_3$ -based PSCs, and the highest PCE achieved by inorganic  $\text{CsSnI}_3$  based

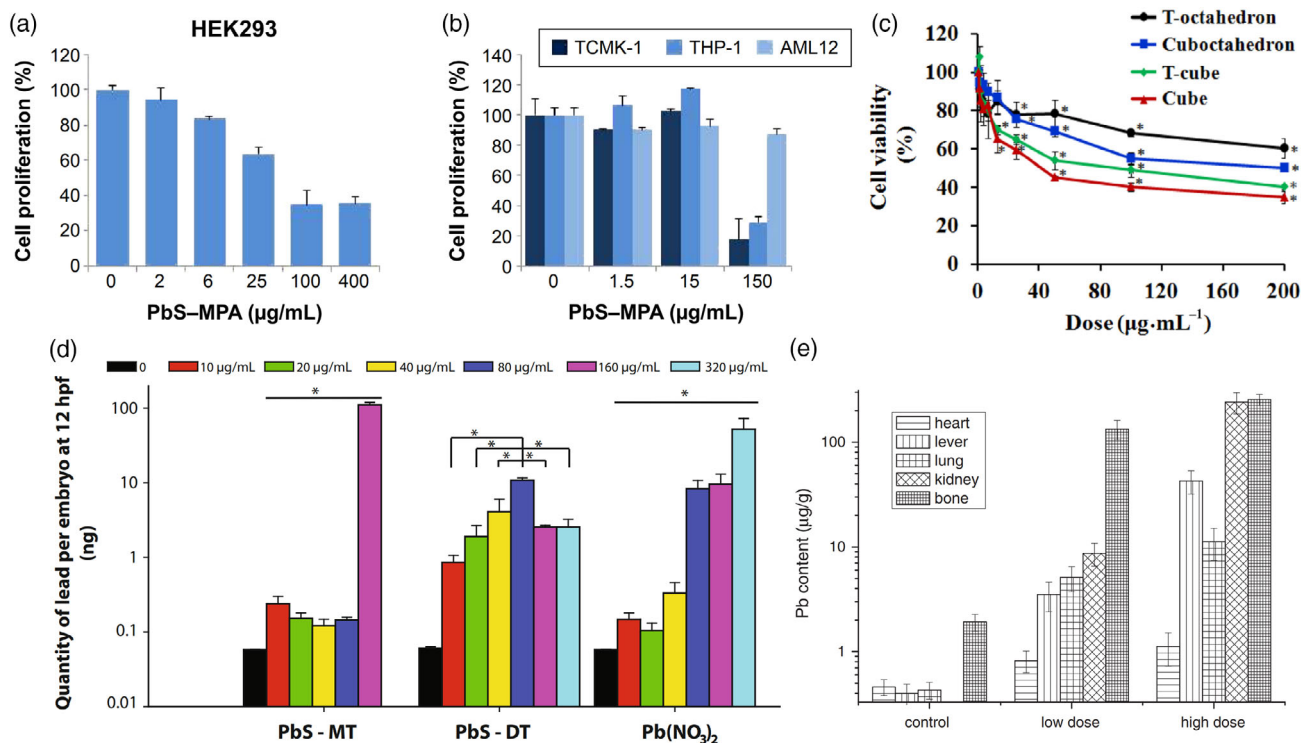


**Figure 10.** Cytotoxicity of PbS-MPA for a) HEK293 cells and b) THP-1, TCMK-1, and AML12 cells. Reproduced with permission.<sup>[83]</sup> Copyright 2015, Dovepress; c) Cytotoxicity of BEAS-2B cells treated with  $\approx 0.4$  to  $\approx 200 \mu\text{g mL}^{-1}$  PbS nanocrystals for 24 h. Reproduced with permission.<sup>[82]</sup> Copyright 2016, Springer; d) Tissue concentration of Pb in embryos exposed to  $0$ – $320 \mu\text{g mL}^{-1}$  solution of PbS-MT, PbS-DT, and  $\text{Pb}(\text{NO}_3)_2$ . Reproduced with permission.<sup>[81]</sup> Copyright 2011, Springer; e) Pb levels in organs of male Sprague–Dawley (SD) rats. Reproduced with permission.<sup>[84]</sup> Copyright 2013, Elsevier.

PSCs has also surpassed 10%.<sup>[96–99]</sup> Nevertheless, the efficiency is still inferior to that of lead-based PSCs. At the same time,  $\text{Sn}^{2+}$  is easily oxidized to  $\text{Sn}^{4+}$  after exposure to air, which leads to a self-doping phenomenon in the crystal, resulting in the degradation of device performance.<sup>[100,101]</sup> It therefore not only increases the harsh requirements for the preparation environment of Sn-based PSCs but also improves the requirements of device encapsulation costs. In general, Pb-based perovskites are irreplaceable as the most promising perovskite PV materials for commercialization.

While maintaining the high efficiency of Pb-based PSCs, some researchers used binary and multi-metal blending techniques to replace Pb ions partially and reduce the Pb content in PSCs. In 2016, Huang et al. prepared a binary cation PSC based on  $\text{MASn}_{0.5}\text{Pb}_{0.5}\text{I}_3$  with a PCE of 13.6% by substituting 50% mol Pb with Sn.<sup>[102]</sup> (Figure 11a) The device performance was improved with the increase of Pb content from 0% to 50%, as shown in Figure 11b, ascribing to the reduced crystallization rate of tin-based perovskite and the compactness of the Sn/Pb binary perovskite film. In 2018, Chen et al. fabricated  $\text{FAPb}_{0.7}\text{Sn}_{0.3}\text{I}_3$ -based PSCs with a PCE of 16.26% through a two-step process.<sup>[103]</sup> With the addition of 0.25 MASCN, the morphology of the perovskite film was tuned and oxidation of  $\text{Sn}^{2+}$  was retarded through coordinated  $\text{SCN}^-$  to  $\text{Sn}^{2+}$ . Liao et al. used  $\text{SnI}_2$  and  $\text{CuBr}_2$  to partially replace  $\text{PbI}_2$  to prepare the Pb–Sn–Cu ternary perovskite film, and the resulting PSC achieved an optimal PCE of 21.08%.<sup>[104]</sup> The roles of Sn and Cu substitution of Pb were found to promote the formation of high-quality ternary perovskite films with full film coverage. (Figure 11c) Meanwhile, Ning tuned the energy level of the HTL and boosted the

performance of Sn–Pb mixed inverted PSCs with a champion PCE to 15.85% based on  $\text{FA}_{0.6}\text{MA}_{0.4}\text{Sn}_{0.6}\text{Pb}_{0.4}\text{I}_3$  perovskite.<sup>[105]</sup> Subsequently, Chen et al. also reported a highly crystallized Pb–Sn hybrid perovskite ( $\text{FA}_{0.7}\text{MA}_{0.3}\text{Sn}_{0.5}\text{Pb}_{0.5}\text{I}_3$ ) by introducing  $[\text{PNA}]\text{BF}_4$  ionic molecule, which functions as an anchoring agent to bond  $\text{Pb}^{2+}$  to the HTL surface (Figure 11d), enabling a mixed Sn–Pb PSCs with a champion PCE of 20.11% and improved thermal and shelf storage stability.<sup>[106]</sup>

From the perspective of Pb–Sn blending, Pb concentration can be reduced effectively while the PCE can be maintained to some extent. Pb–Sn binary metal perovskites can effectively tune the bandgap of perovskite films and be incorporated into high-efficiency PSCs, including tandem devices. However, as the ratio of Sn increases, the stability of Pb–Sn binary perovskites decreases, posing challenges to the fabrication process, encapsulation technologies, and device stability issues. The use of partially substituted Pb to create efficient and stable Sn–Pb hybrid PSCs is an essential direction for future research.<sup>[102,103,107,108]</sup> Although Sn has been proposed to be as hazardous as Pb,<sup>[85]</sup> composition engineering may not be a final solution for Pb toxicity issues. In addition to the research effort in full or partial Pb replacement, Pb reduction materials were introduced in PSC layers, the interlayers, or encapsulation materials in Pb-based PSCs.

### 5.1.2. Additives in PSC Function Layers for Pb Leakage Reduction

*In Perovskite Active Layers:* Various additives, such as phosphonic salts,<sup>[109]</sup> polyamide,<sup>[110]</sup> sulfonic acid,<sup>[111,112]</sup> fullerene,<sup>[113]</sup> fluoro-ine molecule,<sup>[114]</sup> have been incorporated into the active layer and chemically reacted with perovskite materials. These

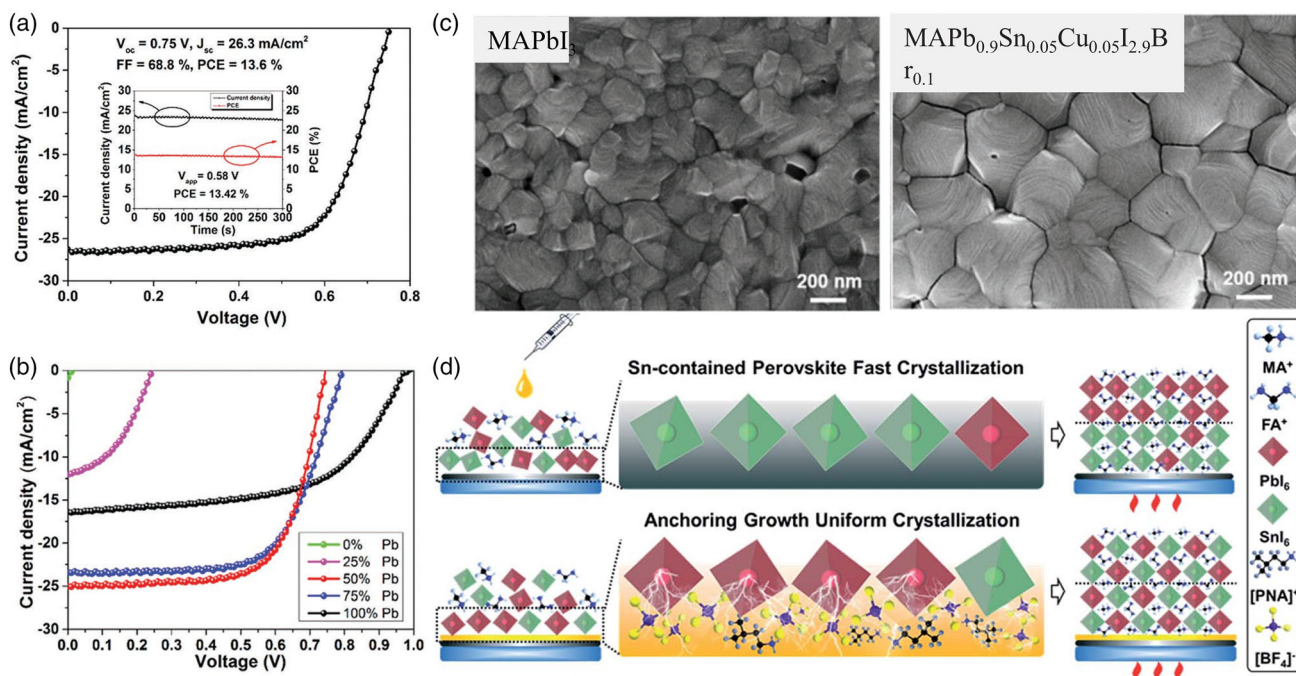


**Figure 11.** a) J–V curve of the best PSC fabricated with the Pb-assisted two-step method. b) J–V curves of PSCs based on perovskite films with different Pb concentrations. Reproduced with permission.<sup>[102]</sup> Copyright 2021, Wiley–VCH GmbH. c) Top scanning electron microscope (SEM) images of  $\text{MAPbI}_3$ , and  $\text{MAPb}_{0.9}\text{Sn}_{0.05}\text{Cu}_{0.05}\text{I}_{2.9}\text{Br}_{0.1}$  perovskite films. Reproduced with permission.<sup>[104]</sup> Copyright 2021, Wiley–VCH. d) The schematic illustration of  $[\text{PNA}]\text{BF}_4$  ionic substrates anchoring growth of mixed Sn–Pb perovskite. Reproduced with permission.<sup>[106]</sup> Copyright 2021, Royal Society of Chemistry.

strategies were proved to effectively immobilize Pb ions and further mitigate  $Pb^{2+}$  leakage while not decreasing the efficiency of PSCs.

Phosphate salts, such as  $(NH_4)_2HPO_4$ , were incorporated into MAPbI<sub>3</sub>-based PSCs by Horváth et al.<sup>[109]</sup> It's interesting to note that phosphate salts don't interact with perovskite and don't modify its advantageous features. Still, they interact with Pb ions under highly humid conditions, creating a highly insoluble complex and preventing  $Pb^{2+}$  leakage. Niu et al. used dormant acrylamide as an additive to the perovskite precursor to mitigate the  $Pb^{2+}$  leakage of PSCs.<sup>[110]</sup> The acrylamide additives may produce chelating polymer networks inside the perovskite layers during annealing. (Figure 12a) As a result, a PCE of 22.1% is attained with a high level of stability ( $T_{80} > 1000$  h). In addition, when the unencapsulated devices are submerged in water, chelating polymer networks capture 94% of the  $Pb^{2+}$  ions. Huang et al. integrated mesoporous sulfonic acid resins into perovskite absorbers to trap Pb ions, increasing the PCE to 20.1% and scaling it up to 16.3% for large-area modules with an aperture area of 60.8 cm<sup>2</sup>.<sup>[111]</sup> As illustrated in Figure 12b,c, the  $Pb^{2+}$  concentration of rainwater from damaged perovskite modules for Device I

without any  $Pb^{2+}$  adsorbents was  $16.0 \pm 0.8$  ppm. In contrast, for Device III with a Pb-adsorbing resin layer beneath the perovskite, it was reduced to  $4.51 \pm 0.68$  ppm. By applying a plastic sheet encapsulation coated with an additional thick layer of Pb-adsorbent resins (device IV), the  $Pb^{2+}$  level was further reduced to 11.9 ppb. Wei et al.<sup>[113]</sup> synthesized a functional fullerene (FPD) with a C<sub>60</sub> cage, a porphyrin ring, and pentafluorophenyl groups in the perovskite precursor. The electron-deficient and pentafluorophenyl groups can suppress ion migration and passivate deep defects, resulting in an FPD-based device with a maximum PCE of 23%. Notably, a water-insoluble complex (FPD–Pb) was produced due to the chelation effect, resulting in a 58.3% reduction in  $Pb^{2+}$  leakage when submerged in water. (Figure 12d) Han et al. included a water-insoluble amphoteric phenyl benzimidazole sulfonic acid (PBSA) in the perovskite precursor.<sup>[112]</sup> The PBSA sulfonic and imidazole rings reacted with  $Pb^{2+}$  to passivate defects, promote crystallization, and constrain  $Pb^{2+}$  leakage. Consequently, the device using 0.3% mol PBSA produced the highest efficiency of 23.27% with low hysteresis and enhanced stability. Additionally, the  $Pb^{2+}$  leakage level decreased from approximately 3.5 to 1 ppm when the

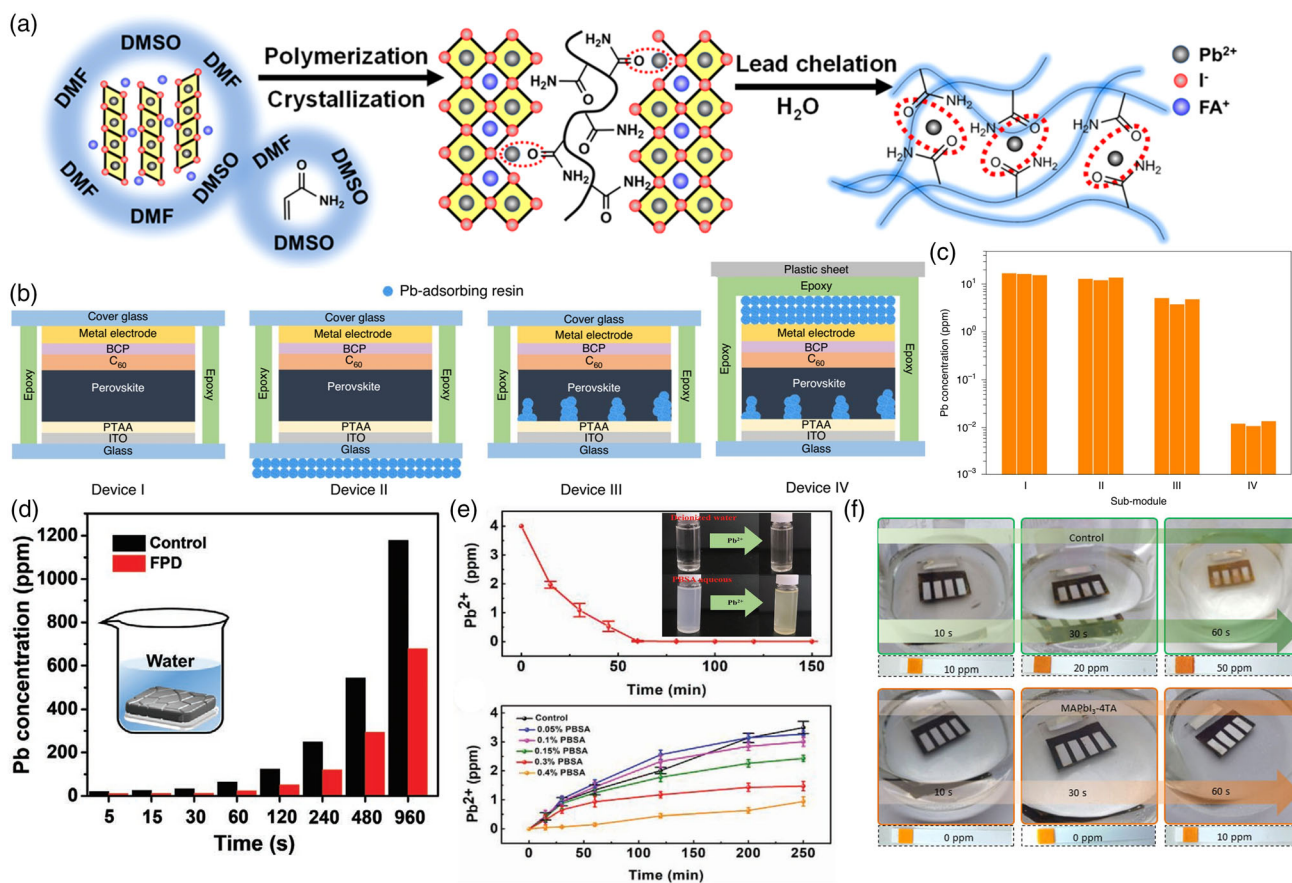


**Figure 12.** a) Illustration of additive-to-polymer transformation in solution (left), solid (middle), and water (right). Reproduced with permission.<sup>[110]</sup> Copyright 2021, American Chemical Society. b) The device architecture of four types of sub-module. c) The Pb concentrations from four types of sub-module, each with three samples tested. Reproduced with permission.<sup>[111]</sup> Copyright 2021, Springer Nature. d) Soaking test for different durations. Reproduced with permission.<sup>[113]</sup> Copyright 2021, Wiley–VCH GmbH. e) Phenyl benzimidazole sulfonic acid (PBSA) powder in 10 mL  $PbI_2$  solution (top); soaking test for unencapsulated devices. Reproduced with permission.<sup>[112]</sup> Copyright 2021, Wiley–VCH GmbH. f) Soaking test for unencapsulated devices with a pH of ≈5.7. Reproduced with permission.<sup>[114]</sup> Copyright 2021, Springer.

unencapsulated device was immersed in deionized (DI) water due to the strong interaction between PBSA molecules and water-soluble  $\text{Pb}^{2+}$  to generate insoluble complexes in water. (Figure 12e). Similarly, Li et al.<sup>[114]</sup> employed a multifunctional regulator, namely 4-[(trifluoromethyl) sulfanyl]-aniline (4TA) to enhance the perovskite crystallization and passivate trapping density, leading to a PCE improvement up to 20.24% with enhanced humidity stability due to the hydrophobic fluorine molecule. Furthermore,  $\text{Pb}^{2+}$  leakage was suppressed due to the formation of the chemical bonds between the aniline of 4TA with  $\text{Pb}^{2+}$  ions. (Figure 12f) Cao et al. implanted poly(butylene adipate-co-terephthalate) polymer (PBAT) in the perovskite film and formed a polymer network that prevented nearly 98% of  $\text{Pb}^{2+}$  from leakage.<sup>[115]</sup>

*In Carrier Transport Layers:* Charge transport layers play significant roles in device performance, including determining charge carrier mobility and protecting the perovskite active layer from the external environments.<sup>[2]</sup> Multifunctional hole-transport materials were developed to regulate the degradation of perovskite and promote  $\text{Pb}^{2+}$  chelation when released from the

perovskite lattice. Alkoxy-PTEG, a conjugated polymeric hole transport material with the ability to chelate  $\text{Pb}^{2+}$  ions, was developed by Lee et al.<sup>[116]</sup> (Figure 13a) It has been demonstrated that the tetraethylene glycol and alkoxy-based groups interact with  $\text{Pb}^{2+}$  ions through chelation. The binding constant ( $K_{\text{binding}}$ ) was determined to be  $2.76 \text{ M}^{-1}$  using proton nuclear magnetic resonance spectroscopy. (Figure 13b) Secondary ion mass spectrometry (SIMS) depth profiling was used to determine the amount of  $\text{Pb}^{2+}$  in the HTL of aged PSCs, proving that  $\text{Pb}^{2+}$  ions were bound to alkoxy-PTEG. (Figure 13c) Dong et al. assembled a series of nanostructured polyoxometalates–metal–organic frameworks (P@Ms) dopants in the HTM of PSCs with improved stability.<sup>[117]</sup> The P@Ms acted as a spider web to trap  $\text{Pb}^{2+}$  ions thereby effectively restricting the migration and leakage of  $\text{Pb}^{2+}$ .

*In Carbon Electrodes:* Carbon electrodes are cheap, stable, inherently water-resistant, and inert to ion migration compared with commonly used Au or Ag electrodes.<sup>[119,120]</sup> The use of carbon electrodes has significantly enhanced the device's stability and shows promise for preventing  $\text{Pb}^{2+}$  leakage.<sup>[119]</sup> Huang et al. integrated cation-exchange resins (CERs) with carbon

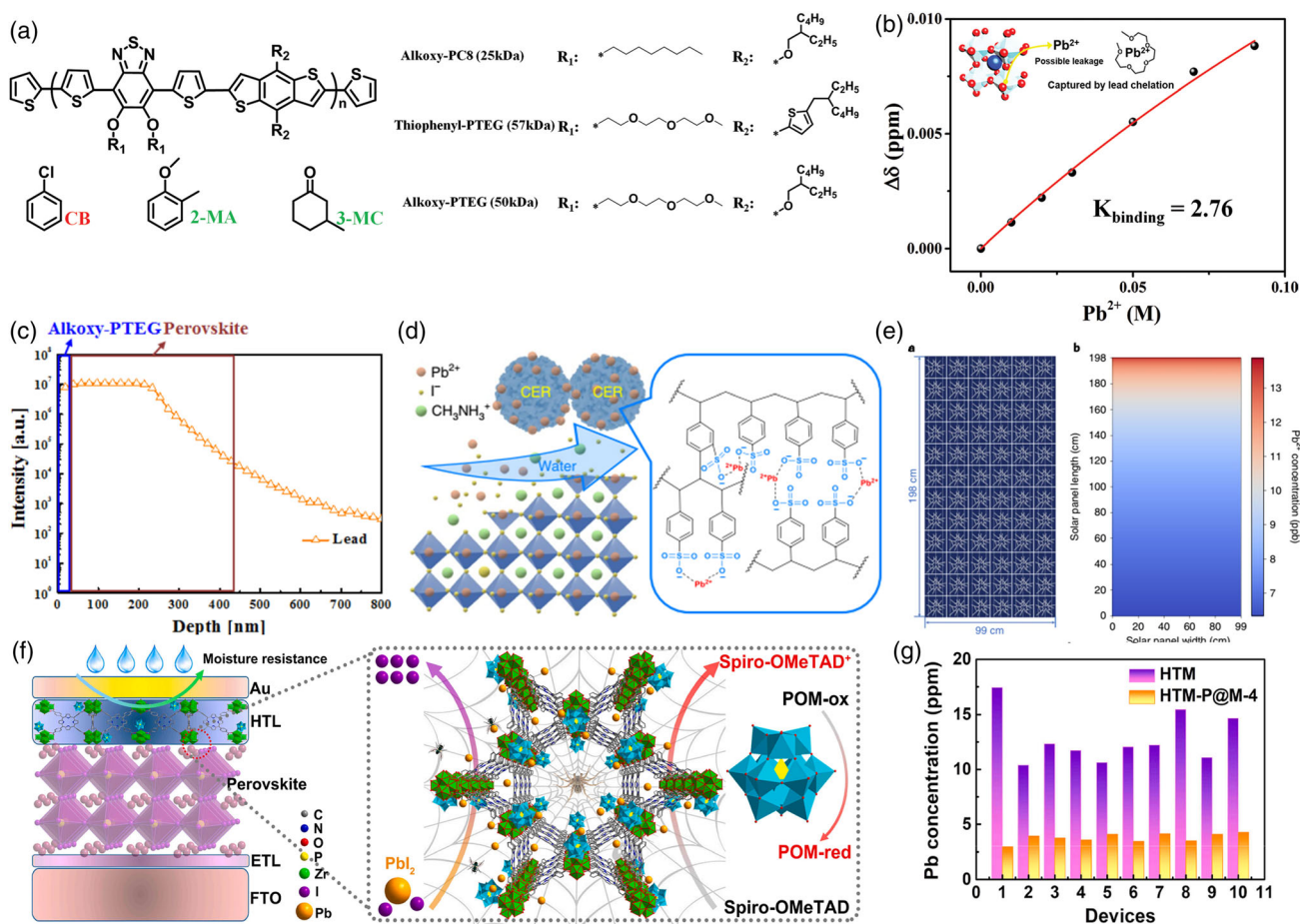


**Figure 13.** a) Chemical structures of alkoxy-PC8, thiophenyl-PTEG, and alkoxy-PTEG. b) Plots of chemical shifts versus  $[\text{Pb}^{2+}]$ . c) Secondary ion mass spectrometry (SIMS) depth profiles, Pb tracking in Alkoxy-PTEG. Reproduced with permission.<sup>[116]</sup> Copyright 2021, Wiley-VCH GmbH. d) Schematic of Pb leakage prevention due to the strong ionic interaction between  $\text{Pb}^{2+}$  ions and sulfonate groups. e) Pb leakage simulation and mapping of the concentration on a large, damaged perovskite solar panel. Reproduced with permission.<sup>[118]</sup> Copyright 2020, Nature. f) The schematic of the positive effects of P@M on the efficiency and stability of devices. g) Pb concentration of the contaminated water detected by inductively coupled plasma-optical emission spectrophotometry (ICP-OES). Reproduced with permission.<sup>[117]</sup> Copyright 2020, Nature.

electrodes for  $\text{Pb}^{2+}$  SEQUESTRation from damaged PSCs (Figure 13d).<sup>[118]</sup> The low-cost and easily integrated CERs can effectively trap free  $\text{Pb}^{2+}$  ions inside PSCs owing to the strong bonding capacity of sulfonate groups. Notably, electrodes mixed with CERs had a negligible negative impact on device efficiency. Further, water dripping tests show that the damaged solar mini-modules with coated CER layers can effectively reduce  $\text{Pb}^{2+}$  leakage by 62-fold to 14.3 ppb in water compared with the mini-modules without CER layers. Further encouraging findings (<7.0 ppb) were achieved from the simulation of damaged carbon perovskite solar panel with a typical size of 198 cm × 99 cm, even under heavy and acidic rainfall (50 mm h<sup>-1</sup>, pH = 4.2) conditions with every mini-module damaged. (Figure 13e)

As shown in **Table 1**,  $\text{Pb}^{2+}$  leakage prevention strategies in PSC layers are summarized. Various test technologies were employed to evaluate the  $\text{Pb}^{2+}$  leakage, including inductively coupled plasma mass spectrometry (ICP-MS),<sup>[109,111,113,118]</sup> atomic absorption flame emission spectrophotometry (FAAS),<sup>[110]</sup> scanning electron microscopy-energy dispersive X-ray spectroscopy (SEM-EDS),<sup>[114]</sup> inductively coupled plasma-optical emission spectrophotometry (ICP-OES),<sup>[109]</sup> and UV-vis absorption spectra.<sup>[116]</sup> Pb-absorbing additives were proved to simultaneously boost the PCE of the device and block  $\text{Pb}^{2+}$  outflow.

### 5.1.3. Interfacial Modification for Pb Leakage Reduction

Interfaces of PSC functional layers are related to surface passivation, carrier dynamics, and defect management, which is essential for improving the performance and long-term stability of the device.<sup>[122]</sup>  $\text{Pb}^{2+}$  leakage was also effectively reduced by adding interfacial modification materials between the perovskite active layer/carrier transport layer (ETL or HTL) and ETL/metal electrode interface.

**Perovskite/HTL Interface:** The perovskite/HTL interface is associated with the electron injection barrier and hole-extraction process, further affecting the device's efficiency and stability.<sup>[122]</sup> Thiol Copper(II) porphyrin was employed to modify the perovskite/HTL surface.<sup>[123–125]</sup> Cao et al. synthesized a tetra-thiol copper porphyrin (CuP) molecule as a perovskite surface modifier and effectively prevented  $\text{Pb}^{2+}$  leakage by the interfacial Pb–S bonds formation.<sup>[123]</sup> The resulting CuP-modified PSCs obtained an enhanced PCE up to 20.7%, while the quantity of  $\text{PbI}_2$  in modified perovskite film is half the amount in pristine perovskite film after 10 min of soaking in water. (Figure 14a) They also introduced a copper porphyrin containing thiol and secondary amine group (Cu-Por) in the perovskite/HTL interface, achieving an enhanced PCE of 21.24% and effectively preventing  $\text{Pb}^{2+}$  leakage in perovskite films.<sup>[124]</sup> (Figure 14b,c) The same group also designed an in situ polymerized zinc porphyrin with carbonyl groups to chelate with Pb ions in perovskite films.<sup>[126]</sup> (Figure 14d) The modified PSCs exhibited a PCE of 20.53% and good light and heat stability due to the passivation effect of ZnP. The UV-vis spectra revealed that the  $\text{PbI}_2$  amount in Zn-por-treated perovskite film was lower than that in the pristine film. (Figure 14e) Phenylbenzimidazole sulfonic acid (PBSA) was also used to modify the perovskite/HTL interface.<sup>[127]</sup> The strong bonds between water-insoluble PBSA and  $\text{Pb}^{2+}$  ions

promote the perovskite surface defects passivation and inhibit Pb leakage. The unencapsulated PBSA-modified device discharged less Pb (<5 ppm) than those without modification when submerged in water. (Figure 14f) Wang et al. introduced the dithiol molecule to passivate surface defects and trap Pb ions.<sup>[128]</sup> Consequently, Pb content from the 1,2-ethanedithiol (1,2-EDT) treated perovskite films was reduced than pristine perovskite films when immersed in DI water and was monitored and recorded as shown in Figure 14g. Chen et al. introduced a chemically stable Dion–Jacobson 2D perovskite of (DOE)PbI<sub>4–x</sub>Cl<sub>x</sub> at the 3D perovskite surface.<sup>[129]</sup> Due to retarded dissolution by the modification layer, the perovskite film avoided drastic structural decomposition when immersed in water. As a result, the modified device showed enhanced PCE performance (23.6%) and operational stability (retain 95% of its initial PCE after 1100 h). Meanwhile, the Pb content of PSCs was dramatically decreased from 231.9 ± 20.1 to 65.2 ± 6.2 ppb by 71.9% when immersed in acid rain, and it exhibited no obvious change after aging for over 1 year. (Figure 14h,i) Wang et al. immobilized lead by doping poly(acrylic acid) grafted carbon nanotubes in perovskite films and reduced about 70% of the  $\text{Pb}^{2+}$  leakage below the hazardous waste limit upon water exposure.<sup>[121]</sup> Zhu et al. introduced an “internal packaging” crosslinked interfacial layer with benzyl acrylate acting as an airtight “protective wall,” which prevented the device from water and oxygen corrosion and lead leakage.<sup>[130]</sup>

**ETL/Perovskite Interface:** The ETM/perovskite interface is crucial for facilitating electron transport, reducing carrier recombination, and regulating perovskite crystallization.<sup>[122]</sup> Meng et al. introduced Diphosphatidyl-glycerol(Di-g) with hydrocarbon chains between ETM/Perovskite interface.<sup>[131]</sup> Due to the bonding between amphipathic Di-g and  $\text{Pb}^{2+}$ , the treated flexible device achieved a PCE of 20.29% and retained 96%  $\text{Pb}^{2+}$  leakage. (Figure 15a,b) Mokhtar et al.<sup>[132]</sup> blended hydroxyapatite NPs into the mesoporous TiO<sub>2</sub> layer to boost the PCE of PSCs up to 20.98%, which also effectively immobilize Pb ions in a hydroxyapatite matrix and promote  $\text{Pb}^{2+}$  leakage SEQUESTRation. (Figure 15c) Zhang et al. prepared amino trimethylene phosphonic acid (ATMP)-K by mixing ATMP and KOH, which was then incorporated in a SnO<sub>2</sub> ETL in PSCs.<sup>[133]</sup> The ATMP-K-modified perovskite/silicon heterojunction tandem solar cells obtained a boosted PCE of 24.75%, and the  $\text{Pb}^{2+}$  concentrations dropped sharply to 50% of the original as Pb ions were captured by ATMP. (Figure 15d) Inspired by the strong adhesion mechanism of mussels, Wang et al. introduced three biological molecules of 3,4-dihydroxyphenylalanine (DOPA), 3,4-dihydroxyphenethylamine (DA), and 3-(3,4-dihydroxyphenyl) propionic acid (DPPA) into the SnO<sub>2</sub>/perovskite buried interface as interfacial linkers, which produced secondary bonding with undercoordinated  $\text{Pb}^{2+}$  defects.<sup>[134]</sup> The DOPA-modified devices exhibited enhanced stability and a high PCE of 21.5%.<sup>[134]</sup> Xu et al. propose an in situ cross-linked polymer (Spiro-NPU) as an internal encapsulating layer in PSCs with enhanced moisture resistance and lead blockage due to the Pb–O interaction.<sup>[135]</sup>

**ETL/Metal Electrode Interface:** Due to their unique frame structures, metal–organic frameworks (MOFs) have been recently investigated as scaffolds and additives/surface modifiers. Wu et al. utilized thiol-functionalized 2D MOFs as an

**Table 1.** Selective studies of Pb<sup>2+</sup> leakage prevention strategies in PSC function layers.

PSC Device Structure	Modifying Material	PCE [%]	Stability	Pb Leakage Test	Pb Reduction	Year	References
In perovskite films							
FTO/ETM/CH <sub>3</sub> NH <sub>3</sub> PbI <sub>3</sub> /HTM/Carbon	Phosphate salts, (NH <sub>4</sub> ) <sub>2</sub> HPO <sub>4</sub>	/	/	Water soaking without damage, with UV-vis absorption, SEM-EDX, ICP-OES, and ICP-MS	perovskite films, 99.97%	2021	[109]
ITO/NiO <sub>x</sub> /PTAA/ Cs <sub>0.05</sub> (FA <sub>0.9</sub> MA <sub>0.1</sub> ) <sub>0.95</sub> Pb(1 <sub>0.5</sub> Br <sub>1</sub> ) <sub>3</sub> /PCBM/BCP/Ag	Polyamide	22.10;15.70 (Mini modules)	T90 > 1,000 h (1 sun, air, 30 °C)	Water soaking without damage, with FAAS	94%	2021	[110]
ITO/PTAA/ MAPbI <sub>3</sub> / C <sub>60</sub> /BCP/Cu	Sulfonic acid resin	Solar cell: 20.6% mini-modules: 16.3%	Continuous operation at 1 sun, 45 °C for 500 h: no notable influence on device stability compared with the pristine counterparts	Dripping water (pH 4.2) onto the broken modules, with ICP-MS	From 16.0 to 4.51 ppm 11.9 ± 1.4 ppb mini-modules: 99.9%	2021	[111]
ITO/SnO <sub>2</sub> / Cs <sub>0.05</sub> FA <sub>0.46</sub> MA <sub>0.49</sub> Pb1 <sub>0.97</sub> Br <sub>0.03</sub> /Spiro/Ag	Fullerene	23%	T80 > 1500 h, no obvious decay after 400 h illumination; T95 > 120 days (ambient, 25 °C, RH 30%)	Water soaking, with ICP-MS	58.3%	2022	[113]
ITO/SnO <sub>2</sub> /FA <sub>0.92</sub> MA <sub>0.08</sub> PbI <sub>3</sub> / Spiro/Au	Phenylbenzimidazolsulfonic acid	23.27; 15.31 (Mini-modules)	The optimized device maintained around 85% of the initial efficiency after 1000 h of storage without encapsulation (ambient, 25 °C RH 30%), the control device about 40%.	Immersed in DI water, with FAAS	71%	2022	[112]
ITO/SnO <sub>2</sub> /MAPbI <sub>3</sub> / Spiro/Ag	4-[(trifluoromethyl)sulfonyl]-anilin	20.24	Maintain 93% of their original efficiency for over 30 days (≈ RH 55%) in air without encapsulation	Immersed in DI water with a pH of ≈5.7 and Pb <sup>2+</sup> ion test paper, with SEM-EDS	In 60 s, 80% 50 days, much	2022	[114]
ITO/NiO <sub>x</sub> /CsMAFA/ PCBM + C <sub>60</sub> /BCP/Cr/Au	(biodegradability) Poly(butylene adipate-co-terephthalate) polymer	22.07% (0.1 cm <sup>2</sup> ), 20.31% (1 cm <sup>2</sup> )	The encapsulated device maintained the initial efficiency of 80% for 3249 h under MPPT and one sunlight illumination	Immersing perovskite films in water for 240 min, with ICP-OES	98%	2022	[115]
ITO/SnO <sub>2</sub> /MAPbI <sub>3</sub> / spiro-MeOTAD/ MoO <sub>x</sub> /Ag	Poly(acrylic acid) grafted carbon nanotubes	21.8%	The modified devices maintained more than 80% of initial efficiency after 1400 h under N <sub>2</sub> atmosphere	Immersing the device in water, with FAAS	≈70%	2022	[121]
In carrier transport layers							
FTO/SnO <sub>2</sub> / Cs <sub>0.06</sub> FA <sub>0.78</sub> MA <sub>0.16</sub> -Pb <sub>0.94</sub> I <sub>2.4</sub> Br <sub>0.48</sub> /Spiro/Au	Alkoxy-PTEG	21.20	In dark with RH of 40–50% at RT: T88 > 30 days at 10 °C: T94 > 4 days	Water soaking, no damage; with UV-vis spectroscopy	Alkoxy-PTEG can capture lead ions at moderate strength	2020	[116]
FTO/TiO <sub>2</sub> /PCBM/FAPbI <sub>3</sub> / Spiro-OMeTAD/Au	Polyoxometalates-metal organic frameworks	21.5%	Retained approximately 85% of the initial PCE value for over 1000 h in ambient conditions	PSCs immersed in water, with ICP-OES	Over 70%	2022	[117]
In carbon electrodes							
Cu-based device: ITO/PTAA/Perovskite/ C <sub>60</sub> /BCP/Cu Carbon-based device: ITO/PTAA/Perovskite/ C <sub>60</sub> /SnO <sub>2</sub> /Carbon Mini-modules: MAPbI <sub>3</sub> Solar cells: Rb <sub>0.05</sub> Cs <sub>0.05</sub> FA <sub>0.85</sub> MA <sub>0.05</sub> PbI <sub>2.85</sub> Br <sub>0.15</sub>	Sulfonic acid resin	18.10 (carbon-based)	Thermal cycling from 40 to 85 °C: no acceleration of the degradation of encapsulated PSCs after 50 cycles	Water soaking; water dripping, glass side damaged; with ICP-MS	Water dripping (pH 4.2) on mini-modules indoor: 84% outdoor: 91%	2020	[118]

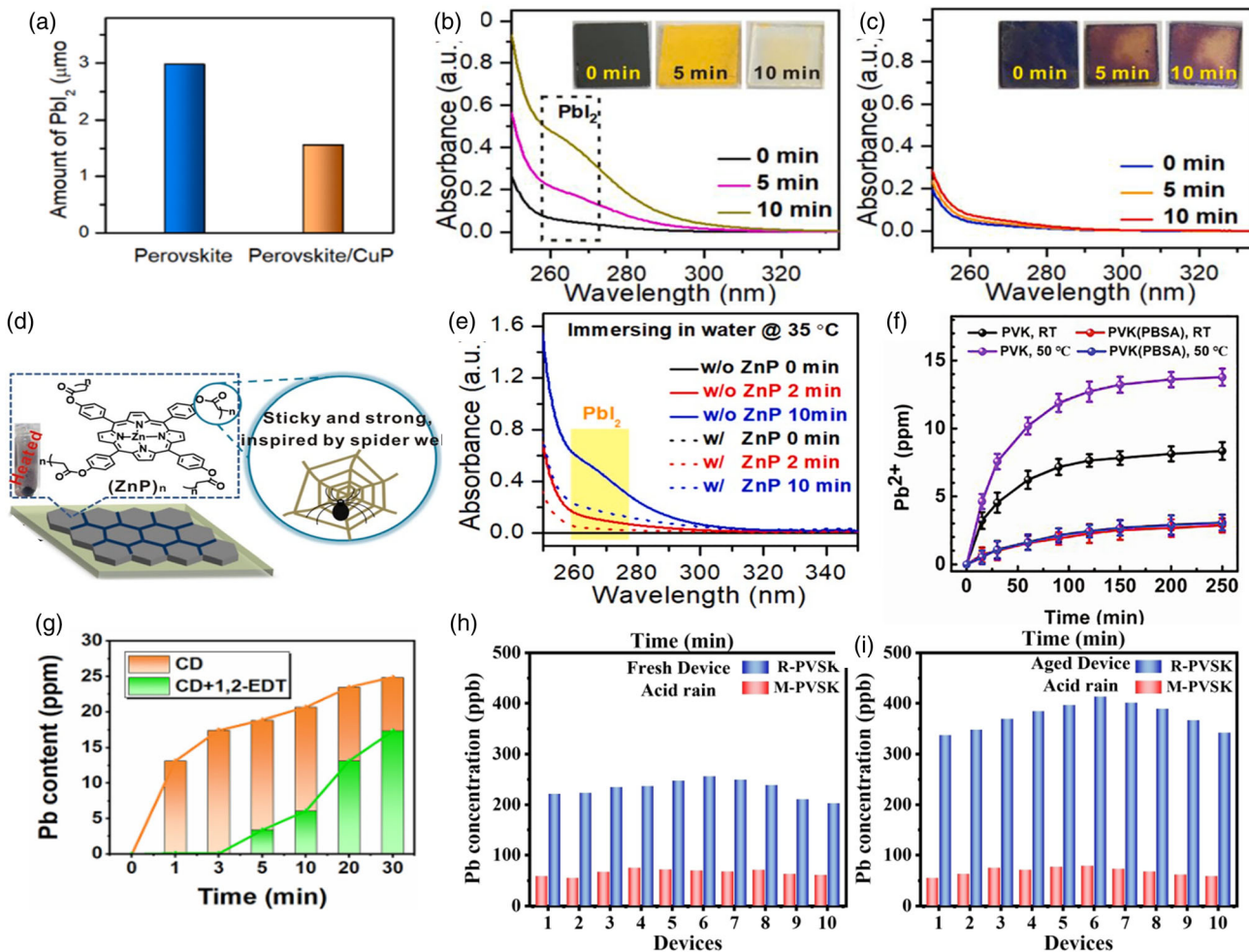


**Figure 14.** a) The leaked amount of Pb<sub>2</sub> after soaking for 10 min. Reproduced with permission.<sup>[123]</sup> Copyright 2021, Elsevier. The film images and UV-vis absorption spectra of the solution by immersing the perovskite films b) without and c) with Cu-Por modification into water at different durations. Reproduced with permission.<sup>[124]</sup> Copyright 2021, Elsevier. d) Chemical structure of ZnP. e) Pb<sup>2+</sup> leakage with ZnP. Reproduced with permission.<sup>[126]</sup> Copyright 2022, Elsevier. f) Pb<sup>2+</sup> concentration by immersing the unencapsulated modules (5 × 5 cm<sup>2</sup>) into 50 mL DI water for 250 min. Reproduced with permission.<sup>[127]</sup> Copyright 2022, Elsevier. g) Pb<sup>2+</sup> content variation when immersing perovskite films in DI water with or without 1,2-EDT treatment. Reproduced with permission.<sup>[128]</sup> Copyright 2022, Wiley-VCH GmbH. The Pb<sup>2+</sup> concentration in the contaminated water under simulated acid rainfall conditions. h) Fresh devices and i) aged devices. Reproduced with permission.<sup>[129]</sup> Copyright 2022, Wiley-VCH GmbH.

electron-extraction layer at the ETL/metal electrode interface.<sup>[136]</sup> With the immobilization of Pb ions via the S–Pb bond, most of the leaking Pb ions were captured from the degraded PSCs by forming water-insoluble solids. (Figure 15e) According to ICP-OES measurements, the Pb<sup>2+</sup> concentration in contaminated water decreased to an average of 7.6 ppm by over 80% of the leaked Pb<sup>2+</sup> ions, which were mostly captured by thiol-containing MOF to form water-insoluble Pb(ii)–ZrL<sub>3</sub> complexes. Superhydrophobic surfaces between the perovskite film and metal electrode are proved as an effective strategy for both efficiency-boosting and Pb reduction.<sup>[137]</sup> The thiol-functionalized superhydrophobic array captured the majority of the uncoordinated Pb<sup>2+</sup> ions via the S–Pb bond. Therefore, Pb<sup>2+</sup> leakage was reduced from 12.28 mg L<sup>-1</sup> (even higher when heating for the control device) to 6–2.05 mg L<sup>-1</sup>, whether heating or not. (Figure 15f).

As shown in **Table 2**, recent advances in Pb<sup>2+</sup> leakage reduction strategies by interfacial modification are summarized. These studies provided further insights into simultaneously developing stable and eco-friendly PSCs via multifunctional interfacial or surface modification.

#### 5.1.4. Encapsulation Absorbers for Pb Leakage Reduction

Encapsulation is an effective way to improve the operational stability of PSCs by enhancing the mechanical strength of modules and preventing environmental factor-related decomposition. To effectively reduce Pb<sup>2+</sup> leakage of PSC devices, some researchers have further adopted device encapsulation technology to prevent Pb<sup>2+</sup> leakage.

Jiang's team reduced Pb<sup>2+</sup> leakage from damaged Pb halide perovskite solar modules by encapsulating PSCs with self-

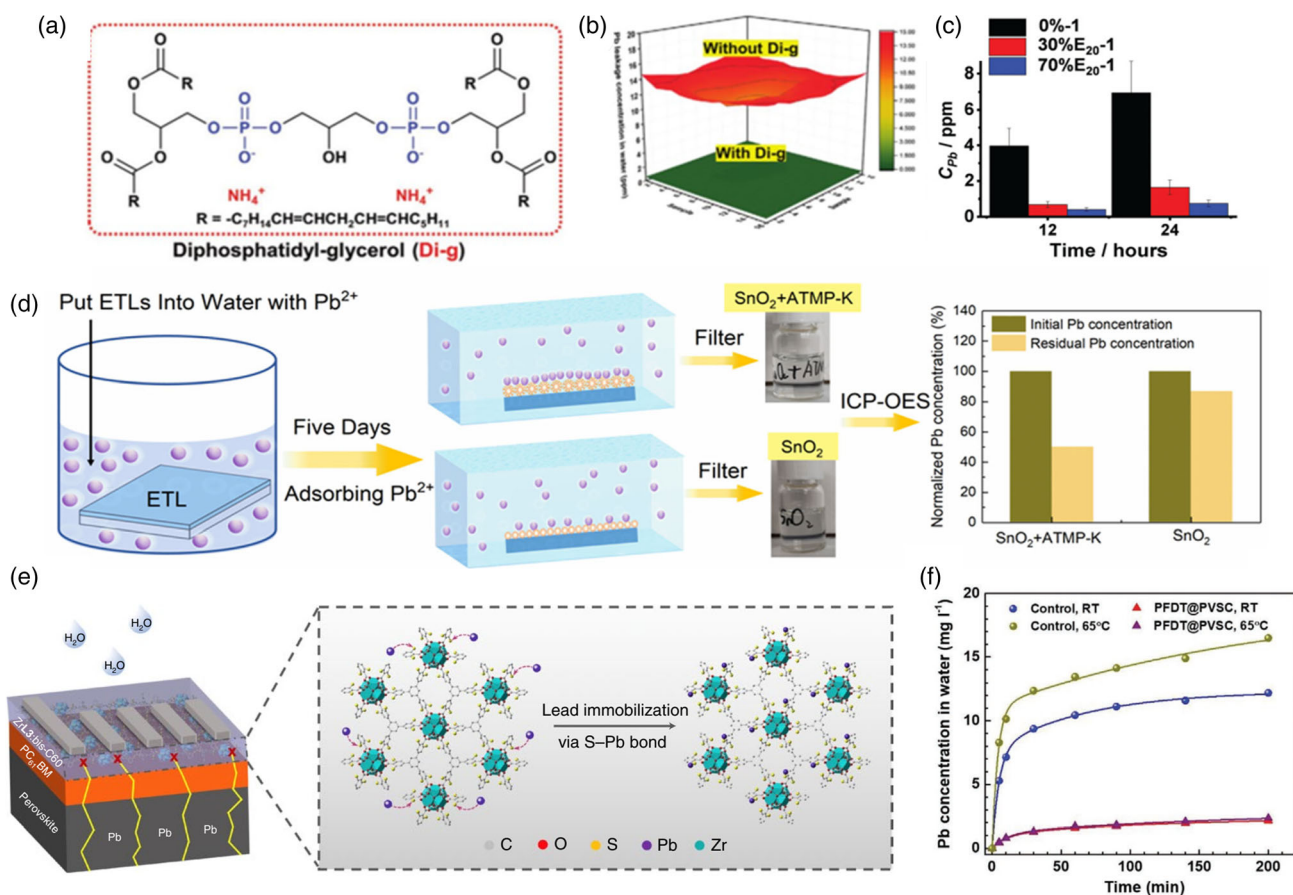


**Figure 15.** a) Molecular structures of diphosphatidyl-glycerol(Di-g). b)  $Pb^{2+}$  leakage distribution in the flexible PSC. Reproduced with permission.<sup>[131]</sup> Copyright 2021, Wiley-VCH GmbH. c)  $Pb^{2+}$  concentration released 12 or 24 h after device breakage. Reproduced with permission.<sup>[132]</sup> Copyright 2021, Royal Society of Chemistry. d) Schematic diagram of  $Pb^{2+}$  adsorption by different electron transport layers (ETLs). Reproduced with permission.<sup>[133]</sup> Copyright 2021, Wiley-VCH GmbH e) Schematic of the immobilization effect of  $ZrL_3$  on  $Pb^{2+}$  ions. Reproduced with permission.<sup>[136]</sup> Copyright 2020, Springer Nature. f) The  $Pb^{2+}$  concentration when soaking both types of devices in water at RT and 65 °C. Reproduced with permission.<sup>[137]</sup> Copyright 2021, Wiley-VCH GmbH.

healing epoxy resin (ER) which has the best sealing effect and its self-healing ability can be triggered by heat provided by sunlight.<sup>[67]</sup> It can effectively reduce  $Pb^{2+}$  exposure to rain, and mitigate  $Pb^{2+}$  leakage from 30 to 0.08  $mg\ h^{-1}\ m^{-2}$  when employed between the perovskite solar module and top glass cover. (Figure 16a) Zhu et al. employed a transparent P, P'-di(2-ethylhexyl)methanediphosphonic acid (DMDP) layer on the glass side and an additional N,N,N',N'-ethyl enediaminetetrakis (methylenephosphonic acid-poly(ethylene oxide) (EDTMP-P EO) layer on the metal-electrode side of the prepared PSCs, which were then covered by the ethylene vinyl acetate (EVA) encapsulation layers.<sup>[138]</sup> (Figure 16b) The Pb-absorbing layers do not negatively impact device PCEs and operation stability while demonstrating excellent on-device SEQUESTration of over 96% of  $Pb^{2+}$  leakage through a chemical absorption approach after a 3 h soaking test in acidic water on damaged PSC devices. (Figure 16c) Subsequently, the same group fabricated  $Pb^{2+}$ -absorbing tapes composed of a standard EVA film and a prelaminated DMDP layer on both sides of PSC devices of n-i-p and p-i-n configurations.<sup>[139]</sup> Consequently, the resulting

device after severe device damage exhibited 99.9%  $Pb^{2+}$  SEQUESTration efficiency upon a 7 day water soaking test. (Figure 16d) Huang reported a self-healable, and Pb-absorbing ionogel-based encapsulation, which effectively increased the long-term stability of PSCs and inhibited  $Pb^{2+}$  leakage.<sup>[140]</sup> (Figure 16e) Zhu et al. used a mixture of sulfonated graphene aerogel and polydimethylsiloxane as a Pb-absorbing encapsulant on both sides of flexible perovskite solar modules.<sup>[141]</sup> Under various simulation conditions (scratching, bending, and thermal cycling), the S-GA/PDMS encapsulant can trap over 99.99% of  $Pb^{2+}$  after 3000 bending circles ( $R = 5\ mm$ ). (Figure 16f) The same group also employed a mixture of a cation-exchange resin (CER) and an ultraviolet resin for encapsulating both rigid and flexible PSCs on the metal side.<sup>[142]</sup> Consequently, more than 90% of  $Pb^{2+}$  from decomposed PSCs and modules may be trapped by the encapsulant through an efficient reaction between CER and  $Pb^{2+}$  under simulated extreme weather conditions.

As shown in Table 3, recent studies of  $Pb^{2+}$  leakage reduction strategies with encapsulation strategies are summarized. Physical encapsulation can protect solar cells from

**Table 2.** Selective studies of Pb leakage prevention strategies by inserting interfacial modifiers.

PSC device structure	modifying material	PCE	stability	Pb <sup>2+</sup> Leakage test	Pb <sup>2+</sup> reduction	year	References
Perovskite/HTL							
FTO/TiO <sub>2</sub> / Cs <sub>0.05</sub> (MA <sub>0.17</sub> FA <sub>0.83</sub> ) <sub>0.95</sub> Pb-(I <sub>0.83</sub> Br <sub>0.17</sub> ) <sub>3</sub> /Sprio/Au	Copper(II) porphyrin	20.70%	T <sub>90</sub> > 1000 h (1 sun, N <sub>2</sub> ); T <sub>90</sub> > 1000 h (85 °C, N <sub>2</sub> ); T <sub>90</sub> > 2000 h (45% RH, N <sub>2</sub> )	Perovskite films, water soaking; UV-vis absorption	For 10 min, 50%	2019	[123]
FTO/TiO <sub>2</sub> / Cs <sub>0.05</sub> (MA <sub>0.17</sub> FA <sub>0.83</sub> ) <sub>0.95</sub> Pb-(I <sub>0.83</sub> Br <sub>0.17</sub> ) <sub>3</sub> /Sprio/Au	Copper(II) porphyrin	21.24%	1 sun, N <sub>2</sub> ; T <sub>90</sub> > 2,000 h; N <sub>2</sub> , 85 °C: T <sub>90</sub> > 2,200 h; RH 45%; T <sub>90</sub> > 3,200 h.	Perovskite films, dip into water, device, UV-vis absorption	effectively inhibited	2021	[124]
FTO/TiO <sub>2</sub> / Cs <sub>0.05</sub> (MA <sub>0.17</sub> FA <sub>0.83</sub> ) <sub>0.95</sub> Pb-(I <sub>0.83</sub> Br <sub>0.17</sub> ) <sub>3</sub> /Sprio/Au	Copper(II) porphyrin	21.76%	1 sun, N <sub>2</sub> ; T <sub>90</sub> > 2,000 h; N <sub>2</sub> , 85 °C: T <sub>90</sub> > 2,000 h; moisture stability: T <sub>90</sub> > 3,200 h, RH 45%; operation stability, 1 sun: T <sub>90</sub> > 1,000 min.	Perovskite films; water soaking; (pH: ≈5.2) UV-vis absorption	Effectively prevented	2021	[125]
FTO/ZnO-MgO-EA <sup>+</sup> /TiO <sub>2</sub> / Cs <sub>0.05</sub> (MA <sub>0.17</sub> FA <sub>0.83</sub> ) <sub>0.95</sub> Pb(I <sub>0.83</sub> Br <sub>0.17</sub> ) <sub>3</sub> /Sprio/Au	Zinc porphyrin	20.53%	Thermal stability: ZnP - treated PSC retained 77% after 900 h, the pristine degraded to 27% after 500 h light stability: the ZnP treated PSC retained 86% after 630 h, and the pristine degraded to 56%	Perovskite films immersed in DI water at 35 °C, UV-vis Absorption	Prevented less Pb <sup>2+</sup> leakage	2022	[126]
ITO/SnO <sub>2</sub> /MAPbI <sub>3</sub> / (DOE)PbI <sub>4-x</sub> Cl <sub>x</sub> / PTAA/Ag	(DOE)PbI <sub>4-x</sub> Cl <sub>x</sub> 2D structure	23.6 %	Retaining 90.7% of their original PCE after 3000 h, RH 25–55% 15–30 °C, only 68.8% for the control device	Immersed in pure/lake/sea water; no damage; ICP-MS	Normal rain, 80% acid rain, 71.9%	2022	[129]
ITO/TiO <sub>2</sub> /FA <sub>0.92</sub> MA <sub>0.08</sub> PbI <sub>3</sub> /Sprio/Au	Phenylbenzimidazole sulfonic acid	24.14%	1 sun, 50 °C: T <sub>90</sub> > 1,130 h, T <sub>80</sub> > 2,000 h	Water soaking, no device damage; FAAS	62.5% (RT) 78.5% (70 °C)	2022	[127]
ITO/SnO <sub>2</sub> /perovskite/ PCBM/Ag	1,2-EDT	20.5%	Maintain 88% of the initial PCE in air for 1005 h	Perovskite films; immersing in DI water	Less Pb <sup>2+</sup> leakage	2022	[128]
ITO/SnO <sub>2</sub> /CsFAMA/ Spiro-OMeTAD/Au	benzyl acrylate	20.86%– 0.07 cm <sup>2</sup> , 16.75%– 24 cm <sup>2</sup> modules	The BzA-based F-PSM exhibits excellent long-term stability (81.0% of the initial PCE after 400 h of 75% humidity testing, 84.5% of the initial PCE after 300 h of light aging at AM 1.5 G)	Immersing the unencapsulated F-PSMs in water f or 240 min; ICP-MS	The control device 12.3 ppm, BzA-based dropped to 2.1 ppm	2022	[130]
FTO/SnO <sub>2</sub> /CH <sub>3</sub> NH <sub>3</sub> PbI <sub>3</sub> /Spiro-OMeTAD/Ag	In situ cross-linked insoluble polymer (Spiro-NPU)	23.26%	No PCE decay after 3000 h in air, 60% RH; maintained over 90% of initial efficiency after 500 h at 85% RH @ 25 °C (or at 55% RH @ 85 °C); retained 97% of the initial PCE after operating at MMP under 1 sun illumination (≈50 °C in N <sub>2</sub> ) for 200 h without encapsulations.	Soaking the CH <sub>3</sub> NH <sub>3</sub> PbI <sub>3</sub> films in DI water, with FAAS	The control device (≈17 ppm, 1 h); the treated device (less than 1 ppm in 20 days and then rised to ≈8 ppm)	2022	[135]
ETL/Perovskite							
ITO/PEDOT: PSS/ (FAPbI <sub>3</sub> ) <sub>1-x</sub> (MAPbBr <sub>3</sub> ) <sub>x</sub> / PC <sub>61</sub> BM/BCP/Ag	Diphosphatidyl- glycerol	20.29%; 15.01% (modules)	Unencapsulated, RH 45%, ambient: T <sub>90</sub> > 60 h	Water soaking (pure, pH 4.5 and 9.3); no device damage; PB-2 A water quality tester	95.7% (pure water) 95.6% (pH 4.5) 94.7% (pH 9.3)	2021	[131]
FTO/TiO <sub>2</sub> /(FAPbI <sub>3</sub> ) <sub>1-x</sub> (MAPbBr <sub>3</sub> ) <sub>x</sub> /Sprio/Au	Hydroxyapatite	20.98%	Ambient conditions: T <sub>85</sub> > 38 days	Water soaking, device front and back sides smashed; a Pb ion-selective electrode	94.6%	2021	[132]

**Table 2.** Continued.

PSC device structure	modifying material	PCE	stability	Pb <sup>2+</sup> Leakage test	Pb <sup>2+</sup> reduction	year	References
ITO/SnO <sub>2</sub> / Cs <sub>0.22</sub> FA <sub>0.78</sub> Pb (Br <sub>0.2</sub> I <sub>0.8</sub> ) <sub>3</sub> /Spiro/Au	Amino trimethylene phosphonic acid	23.52%	Ambient conditions, RH30%–50%: T90 > 1,200 h; N <sub>2</sub> , without any light: T93 > 1,000 h	Water soaking (pH 6.2); no device damage; ICP-OES	91.1%	2021	[133]
ITO/SnO <sub>2</sub> / (MA <sub>0.8</sub> FA <sub>0.2</sub> ) PbI <sub>3</sub> /Spiro-OMeTAD/Au	3,4-DOPA	21.5%	The unencapsulated devices maintain 85% of their initial performance after 55 days in air (RH≈15%, RT)	/	/	2022	[134]
<b>ETL/Metal Electrode</b>							
ITO/PTAA/ Cs <sub>0.05</sub> (FA <sub>0.85</sub> MA <sub>0.15</sub> ) <sub>0.95</sub> Pb(I <sub>0.85</sub> Br <sub>0.15</sub> ) <sub>3</sub> / PC <sub>61</sub> BM/BCP/Ag	MOF	22.02	Encapsulated in RH 75% ambient: T90 > 1,000 h; operation stability at 1 sun in N <sub>2</sub> at 85 °C without UV filter: T92 > 1,000 h	Water soaking (pH 5.6); no device damage; ICP-OES	80.2%	2020	91 <sup>[136]</sup>
FTO/NiO <sub>x</sub> /Cs <sub>0.05</sub> (FA <sub>0.85</sub> MA <sub>0.15</sub> ) <sub>0.95</sub> Pb(I <sub>0.85</sub> Br <sub>0.15</sub> ) <sub>3</sub> / PC <sub>61</sub> BM/BCP/Ag	H, H, H, H-perfluorodecanethiol	21.79	Operation stability at 1 sun in N <sub>2</sub> at 85 °C without UV filter: T90 > 500 h; unencapsulated in RH 85% ambient: T90 > 500 h	Water soaking (pH 5.5); no device damage; ICP-MS	From 12.28 mg L <sup>-1</sup> (higher when heating) to 6–2.05 mg L <sup>-1</sup> no matter heating or not	2021	92 <sup>[137]</sup>

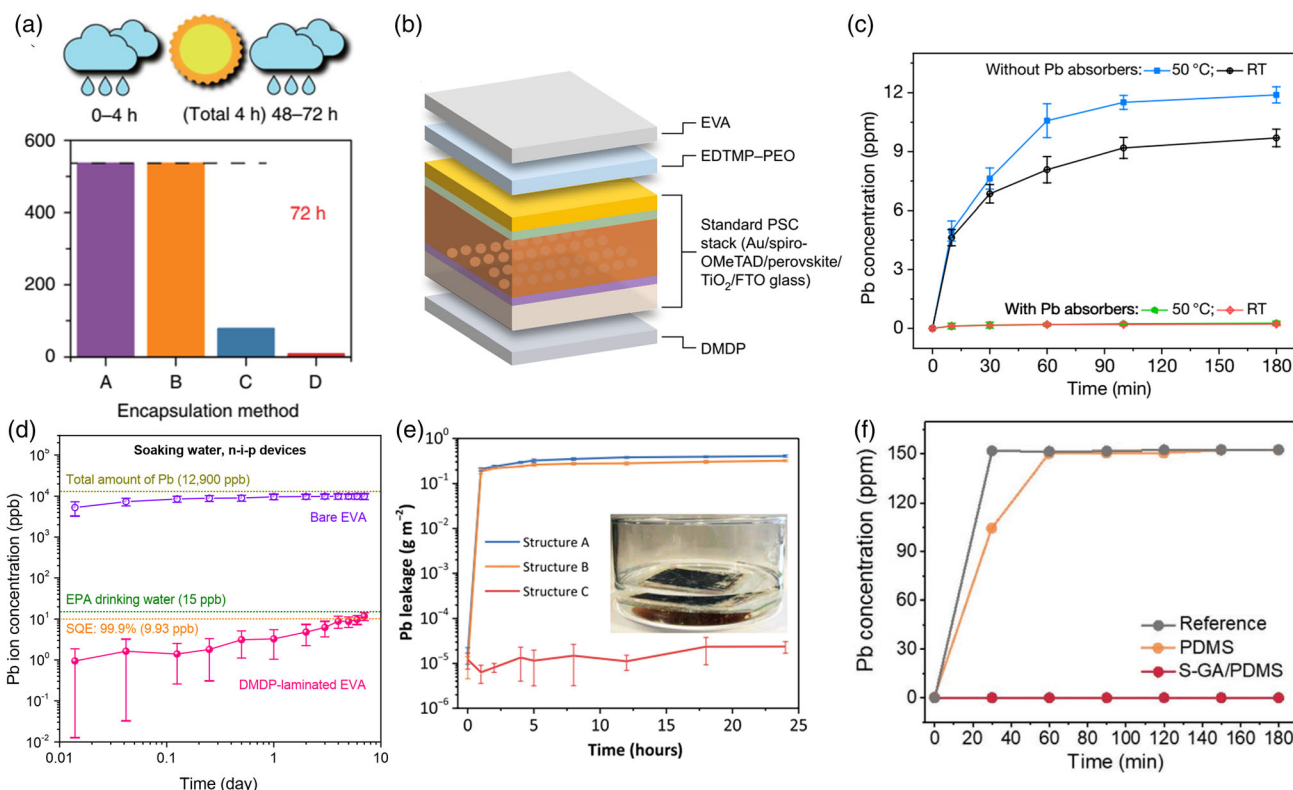


**Figure 16.** a) Pb<sup>2+</sup> leakage with four encapsulation methods when it rains for the first 4 h, is sunny for 4 h in total and rains again starting at 48 h for 24 h (a total of 72 h). Reproduced with permission.<sup>[67]</sup> Copyright 2019, Springer Nature. b) Illustration of adding Pb-absorbing materials on both sides of a standard n-i-p PSC. c) Pb<sup>2+</sup> SEQUESTration for damaged PSCs with and without the Pb-absorbing layers. Reproduced with permission.<sup>[138]</sup> Copyright 2020, Springer Nature. d) Pb<sup>2+</sup> concentration of damaged n-i-p PSCs encapsulated by bare ethylene vinyl acetate (EVA) film and P, P'-di (2-ethylhexyl)methanediphosphonic acid (DMDP)-laminated EVA tapes after a 7 day water-soaking test. Reproduced with permission.<sup>[139]</sup> Copyright 2020, Springer Nature. e) Water soaking test for damaged minimodules. Reproduced with permission.<sup>[140]</sup> Copyright 2021, American Association for the Advancement of Science. f) Pb<sup>2+</sup> leakage of flexible modules without and with different encapsulants after 3000 bending circles (R = 5 mm). Reproduced with permission.<sup>[141]</sup> Copyright 2021, Wiley-VCH GmbH.

**Table 3.** Selective studies of Pb<sup>2+</sup> leakage prevention strategies in encapsulation layers.

PSC Device Structure	Modifying Material	PCE	Stability	Pb <sup>2+</sup> Leakage Test	Pb <sup>2+</sup> Reduction	Year	References
FTO/c-TiO <sub>2</sub> /Cs <sub>0.07</sub> FA <sub>0.93</sub> PbI <sub>3</sub> /spiro- MeOTAD/Au	Epoxy resin	Mini-modules: 14.3%	Not reported	Water dripping (ph 4.2) Glass side damaged	Water-dripping: 98.1% First dripping, heating at 45 °c for 4 h, then water dripping for a second time: 99.8% First heated at 45 °c for 4 h and then water dripping: 99.5%	2019	[67]
ITO/TiO <sub>2</sub> /(CsPbI <sub>3</sub> ) <sub>0.05</sub> (FAPbI <sub>3</sub> ) <sub>0.85</sub> (MAPbBr <sub>3</sub> ) <sub>0.15</sub> /Sprio/Au	EDTMP-PEO DMDP	Reverse: 20.12% Forward: 20.27%	Continuous operation at 1 sun simulated illumination intensity in the air at about 50 °c t80 > 500 h	Water soaking/ dripping; front and back encapsulation cut and substrate smashed; faas	In water 97.7% at rt 97.8% at 50 °c in water (ph 4.2) 96.1% at rt 97.7% at 50 °c	2020	[138]
n-i-p device: FTO/TiO <sub>2</sub> / (CsPbI <sub>3</sub> ) <sub>0.05</sub> (FAPbI <sub>3</sub> ) <sub>0.85</sub> (MAPbBr <sub>3</sub> ) <sub>0.15</sub> /Sprio/Au; p-i-n device: ITO/PTAA/(CsPbI <sub>3</sub> ) <sub>0.05</sub> (FAPbI <sub>3</sub> ) <sub>0.8</sub> (MAPbBr <sub>3</sub> ) <sub>0.15</sub> /C <sub>60</sub> / BCP/Ag	DMDP	n-i-p reverse: 21.08% forward: 21.22%	T80 > 800 h	Water soaking (ph 4.2); dripping; front and back encapsulation cut and substrate smashed; FAAS and ICP-MS	In water 99.9% at RT (n-i-p) 99.9% at RT (p-i-n)	2021	[139]
ITO/PTAA/(FA <sub>0.92</sub> MA <sub>0.08</sub> ) <sub>0.9</sub> Cs <sub>0.1</sub> Pb(I <sub>0.92</sub> Br <sub>0.08</sub> ) <sub>3</sub> /C <sub>60</sub> / BCP/Cu	Ionogel	20.68 (Rigid device); 14.98 (Flexible modules)	RH 85%, 85 °C: T95 > 1,000 h thermal cycling from 40 to 80 °C: 3.9% efficiency loss after 210 cycles	Water soaking; water dripping glass side damaged; ICP-MS	>99.9%	2021	[140]
ITO/PTAA/ FA <sub>0.92</sub> MA <sub>0.08</sub> ) <sub>0.9</sub> Cs <sub>0.1</sub> Pb(I <sub>0.92</sub> Br <sub>0.08</sub> ) <sub>3</sub> / C <sub>60</sub> /BCP/Ag	Sulfonated graphene aerogel	0.68 (Rigid device); 14.98(Flexible modules)	in ambient air (25 °C, RH40%–50%) : T95 > 500 h in ambient air (RH 40–50%, 25 °C) under 30 W LED illumination for 7 days: no obvious degradation	Water soaking; water dripping (pH 4.2) front and back encapsulation film cut and substrate cut	Dripping water >99.99% at RT in water >99.99% at 85 °C (pH 4.2)	2022	[141]
ITO/PTAA/ FA <sub>0.92</sub> MA <sub>0.08</sub> ) <sub>0.9</sub> Cs <sub>0.1</sub> Pb(I <sub>0.92</sub> Br <sub>0.08</sub> ) <sub>3</sub> /C <sub>60</sub> / BCP/Ag Mini-modules:ITO/ PEDOT: PSS/ FA <sub>0.92</sub> MA <sub>0.08</sub> ) <sub>0.9</sub> Cs <sub>0.1</sub> Pb(I <sub>0.92</sub> Br <sub>0.08</sub> ) <sub>3</sub> / PC <sub>61</sub> BM/BCP/Ag	Mixture of CER and ultraviolet resin	21.00; 13.46 (Flexible mini modules)	No obvious degradation for 500 h in air	Water soaking and dripping (ph 4.2); glass side damaged; ICP-OES	Dripping water: 93.5% at RT in water: 97.3% at RT Acid water (ph 4.2): 98%	2022	[142]

environmental degradation and improve mechanical strength against external impact. These results revealed that applying lead-absorbing materials in physical encapsulation is an effective technique to further enhance the operational stability and minimize Pb<sup>2+</sup> leakage from both rigid and flexible PSCs or modules. However, these approaches either needs additional processing procedures for key components of PSCs, or necessitate more encapsulation procedure and materials which would increase

the cost of encapsulation techniques. Consequently, these additional alterations might make it more difficult to fabricate and configure devices. Furthermore, the optical characteristics (i.e., transmission) of encapsulation or lead-absorbing materials, are one of the most important factors, which may potentially impede device performance and scale-up. Consequently, it is of great significance to modulate the material design and device architecture for encapsulating PSC devices with minimal Pb<sup>2+</sup>

leakage and enhanced device performance and stability. More efforts are required to develop encapsulation techniques or lead-absorbing encapsulation materials which are more efficient, easily integrated, cost-effective, and environmentally friendly.

## 5.2. Toxicity reduction strategies for Pb-Based QDSCs

Studies have shown that the surface physicochemical properties, size of QDs, and aggregation state are the key to their toxicity.<sup>[18,143]</sup> In recent years, several groups have been working on surface modifiers to reduce the toxicity of QDs with core-shell structure or ligand exchange techniques.<sup>[144]</sup>

### 5.2.1. Core–Shell structure

The hybrid core/shell configuration is a useful approach to modifying the size and surface toxicity of QDs by enhancing biocompatibility and stability.<sup>[143]</sup> Currently, the most widely studied QDs are core–shell cadmium (Cd)-based QDs in the biomedical fluorescent imaging and the QD display industry, with CdSe/CdTe as the core and ZnS/ZnSe as the surface layer.<sup>[145]</sup> This structure not only gives high luminescence yields and good photochemical stability, but also prevents toxicity due to Cd leakage. In core–shell QDs, the surface properties are mainly related to the molecules covering their shell surfaces, instead of the QD-core materials.<sup>[73,146]</sup> The PbS/PbSe core QDs may exhibit lower toxicity when coated with non-toxic shell materials. Boercker et al. synthesized PbS/ZnS core/shell nanocrystal which provides a less toxic shell layer with controlled thickness.<sup>[147]</sup> However, with the addition of a monolayer ZnS shell, the  $1S_h$ – $1S_e$  absorbance and photoluminescence (PL) peak energies red shifted, and the PL lifetime and quantum yield are also reduced possibly due to nonradiative defect states at the PbS/ZnS interface. Thus, the less hazardous shell not only stabilizes the PbS surface mechanically, but also affects the intrinsic properties of core materials and there are still considerable challenges in the material design of QDs toward an environmentally friendly direction, meanwhile, preserve the QDs excellent optoelectronic properties.

### 5.2.2. Ligand exchange technique

Currently, solution-phase ligand exchange is the most preferred technique for producing the active layers in high-performance PbS QDSCs. PbS QDs are typically capped with long-chain oleic acid (OA) ligands, which passivate the surface of QDs and achieve high stability and monodispersity, however, it may decrease charge conductivity inside the photoactive layer and thus result in reduced QDSC performance.<sup>[148,149]</sup> Therefore, OA ligands were replaced with short-chain Pb-based capping ligands (e.g.,  $PbX_2$ ,  $X = Br, I$ ) to boost the PCE of QDSCs<sup>[150]</sup>, which means extra toxic reagents are needed. Moody et al. introduced a solution phase ligand exchange method with a Pb-free tetrabutylammonium iodide (TBAI) ligand source for the highest performance QDSCs.<sup>[72]</sup> Compared to Pb-based methods, lower material requirements and a nearly 250-fold reduction in  $Pb^{2+}$  waste were demonstrated. Notably, the treated unencapsulated

PbS QDSCs leached less  $Pb^{2+}$  than the limitations of the U.S. Environmental Protection Agency and hence do not need end-of-life hazardous disposal.

Considering the diversity of QDs, and the complex  $Pb^{2+}$  leakage related parameters, mitigating the environmental risk posed by  $Pb^{2+}$  leakage can be a significant challenge to the commercialization of Pb-based QD PV technologies.

## 6. Perovskite solar cell treatment and recycling

For end-of-life PSCs waste, the traditional disposal methods include landfill, incineration, and recycling.<sup>[38,151]</sup> As most PSC devices utilize costly and poisonous materials, recycling Pb-based PSCs has enormous economic and ecological benefits. Hence, the development of efficient treatment and recycling methods for extracting Pb components from PSCs are widely studied.<sup>[38,152,153]</sup> The related methods can be principally categorized as two types of physicochemical treatment for reproducing Pb-containing raw materials and in situ recycling of  $PbI_2$ .

### 6.1. Physicochemical treatment

Physicochemical treatment uses waste PSCs to reproduce the Pb containing raw materials via physicochemical methods, including solvent extraction, chemical precipitation, and electrochemical deposition.<sup>[152–157]</sup> Poll et al. demonstrated the recycling of Pb from hybrid organic–inorganic perovskites by dissolution and selective electrodeposition using a deep eutectic solvent based electrochemical recycling process.<sup>[152]</sup> The extraction ratios of Pb from deep eutectic solvent of  $MAPbI_3$ ,  $MAPbI_3$ , and  $MAPbI_{3-x}Cl_x$  were up to 99.7, 98.7, and 99.8%, respectively. Kardo et al. developed a selective recycling process for PSC devices.<sup>[153]</sup> Ethanol, methanol, water, and isopropanol were used to dissolve  $CH_3NH_3PbI_3$ , and dimethylformamide (DMF) was used to remove  $PbI_2$  completely. The fastest observed conversion from  $CH_3NH_3PbI_3$  to  $PbI_2$  was achieved using methanol, followed by DI water. Relative Pb content in methanol and DMF were 7.1% and 92.9%, respectively. Feng et al.<sup>[155]</sup> reported a close-loop recycling strategy (Figure 17) to extract high-purity  $MAPbI_3$  crystals from PSCs using N-butylamine (BA) as a solvent, with a Pb recovery rate of 98.9%. And the highest PCE of the recycled PSC is 17.95%, which is better than that of the devices made of fresh materials. Park et al.<sup>[156]</sup> synthesized a new adsorbent, Fe-coated hydroxyapatite ( $Ca_{10}(PO_4)_6(OH)_2$ , HAP), for both separation and recovery of Pb from PSC pollutants. Nealy 99.99% of Pb was removed by adding 50 mg HAP/Fe composite to 20 mL of 2 mM  $PbI_2$ /DMF and typical perovskite composed of  $PbI_2$ , methylammonium iodide, and DMF. Hong et al.<sup>[157]</sup> synthesized a novel  $Pb^{2+}$  adsorbent-whitlockite ( $Ca_{18}Mg_2(HPO_4)_2(PO_4)_{12}$ ), with an excellent  $Pb^{2+}$  absorption capacity of  $2339 \text{ mg g}^{-1}$ . Moreover, absorbed  $Pb^{2+}$  ions can be recycled as high-purity  $PbI_2$  powder, as the precursor of PSCs, and its PCE achieved an average of 19%.

### 6.2. In Situ recycling

In situ recycling is to recycle  $PbI_2$  from pristine PSCs and regenerate new devices in situ.<sup>[158–161]</sup> Xu et al. established a method

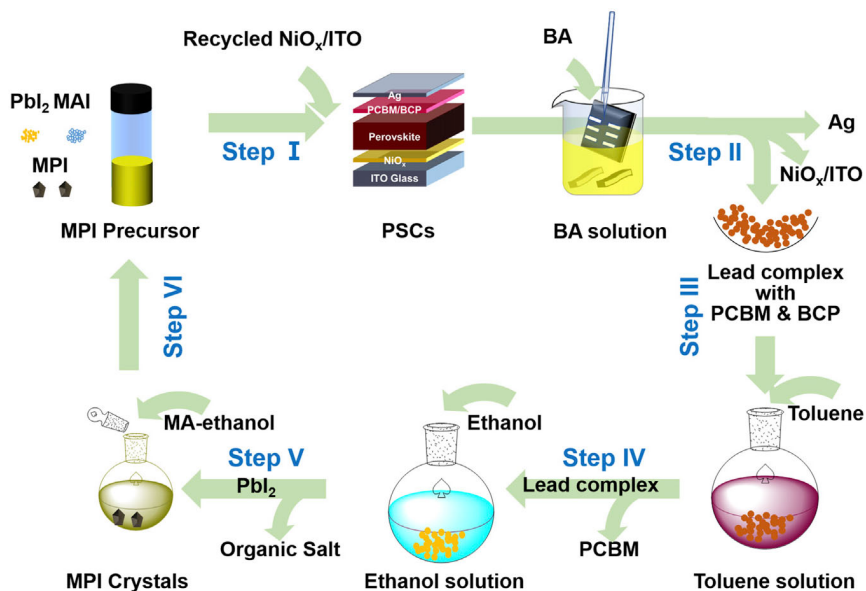


**Figure 17.** Schematics of the closed-loop recycling process. Reproduced with permission.<sup>[155]</sup> Copyright 2021, Elsevier.

for in situ recovery of  $\text{PbI}_2$  from thermally decomposed  $\text{CH}_3\text{NH}_3\text{PbI}_3$  perovskite film for the regeneration of high-efficiency PSCs.<sup>[158]</sup> The performance of regenerated PSC presented a high PCE efficiency of 14.84%. Furthermore, Huang et al. reported a rejuvenation strategy for perovskite crystals regeneration by MAI treatment after 60 days of exposure to ambient air with a relative humidity of 50%.<sup>[159]</sup> The rejuvenated PSC shows a PCE efficiency of 11.6%. Chhillar et al. demonstrated the recycling of  $\text{PbI}_2$  from degraded perovskite film and developed a process for converting  $\text{PbI}_2$  perovskite films by introducing MAI.<sup>[161]</sup> This study demonstrated that recovered  $\text{MAPbI}_3$  films could maintain both optoelectronic properties and crystal structure. Zhang et al. demonstrated Pb recycling and recovery from carbon-based PSCs by the dissolution-precipitation method.<sup>[162]</sup> HI solution was added in DMF dissolved  $\text{MAPbI}_3$  solution for  $\text{PbI}_2$  formation, with a calculated Pb recovery rate of 95.7%. The recovered  $\text{PbI}_2$  was used to fabricate a carbon-based PSC with a PCE of 11.36%. Hong et al. demonstrated a different route to regenerate the degraded PSCs by purging  $\text{CH}_3\text{NH}_2$  gas into the decomposed  $\text{CH}_3\text{NH}_3\text{PbI}_3$  devices.<sup>[160]</sup> And the efficiency of encapsulated PSCs after two cycles of photodegradation-recovery treatment can still reach 91% of the original devices. Ren et al. indicated that  $\text{PbI}_2$  can be recycled through ion exchange by zeolite, and the synthesized  $\text{FAPbI}_3$  based on recycled  $\text{PbI}_2$  showed a stable output PCE of 21.0%.<sup>[163]</sup> Wang et al. reported a one-key-reset method for recycling whole PSCs by dissolving perovskite crystals in a nonionic solvent system consisting of methylamine solution and acetonitrile, the recycled devices exhibited a PCE of  $\approx 20.30\%$ .<sup>[164]</sup>

Overall, the Pb from Pb-based PSCs can be recycled and reused as either  $\text{PbI}_2$ <sup>[160,161]</sup> and other Pb-containing products.<sup>[152]</sup> The efficiency of regenerated PSCs by recycled  $\text{PbI}_2$  can compete with the devices fabricated with fresh materials. More importantly, the recycling and reuse of Pb from PSCs are proved to be an effective strategy for avoiding Pb waste

and preventing Pb contamination at this stage. Tian et al. revealed that the conduction of recycling strategies of PSCs could lead to a decrease in energy payback time and a reduction of greenhouse gas emission factor.<sup>[165]</sup> Therefore, the development of efficient Pb recycle technology for PSCs is obviously beneficial to life cycle management and practical application of Pb-based PSCs. However, the experimental experiences on the PSCs recycling technologies obtained should be adapted to large-scale industrial production. Furthermore, the total cost of PSCs recycling technologies, including materials, synthesizing, etc. should be calculated for the commercial regeneration of PSCs. Finally, the development of lead recycling technology for regenerating PSCs with high efficiency and long-term stability still needs further improvement.

## 7. Conclusion

Despite the excellent performance of emerging Pb-based solar cells,  $\text{Pb}^{2+}$  toxicity is a critical obstacle to its future applications and eco-friendly development. The potential environmental impacts on air, soil, and groundwater, and the ecotoxicity and bioavailability of  $\text{Pb}^{2+}$  leakage to soil plants, bacteria, animals, and human cells were highlighted in this review. However, the understanding of the long-term environmental impact of Pb-based solar cells is not yet fully established, and there is limited research on the bioavailability of Pb-based solar cells compared to other sources of Pb pollutants. Further research is needed to assess the actual on-site  $\text{Pb}^{2+}$  leakage from Pb-based solar cells to ecosystems, including surface and underground water, different types of soil, and air. Up to now, multiple strategies have been employed to achieve both  $\text{Pb}^{2+}$  leakage reduction and performance enhancement. However, challenges still exist toward commercialization, such as adapting lab experiences of  $\text{Pb}^{2+}$  reduction and recycling technologies to large-scale

industrialization and economic calculation of Pb<sup>2+</sup> management processes. Despite the strategies proposed here being still in the infancy stage, we anticipate they will benefit the development of sustainable Pb management of Pb-based solar cells. Furthermore, lead removal and recovery through biological and physiochemical techniques (e.g., precipitation, adsorption, ion exchange, membrane, electrochemical reduction) have been extensively investigated in the field of environmental management of wastewater, sludge, and soil, which is prospective in the field of managing Pb toxicity in Pb-based solar cells.

## Acknowledgments

X.L. and D.Y. contributed equally to this work. This research was supported by the National Natural Science Foundation of China (22106021, 61704027), the Guangdong Basic and Applied Basic Research Foundation (2021A1515012372), Research Fund of Guangdong-Hong Kong-Macao Joint Laboratory for Intelligent Micro-Nano Optoelectronic Technology (No. 2020B1212030010), Engineering and Physical Sciences Research Council (EPSRC, EP/V039717/1), the Royal Society IEC\NSFC \211201-International Exchanges 2021 Cost Share (NSFC), Royal Society of Chemistry (E21-9668828170) and AXA Research Fund.

## Conflict of Interest

The authors declare no conflict of interest.

## Keywords

ecotoxicity, Pb-based photovoltaics, sustainability

Received: July 29, 2022  
Revised: September 9, 2022  
Published online:

- [1] G. E. Eperon, S. D. Stranks, C. Menelaou, M. B. Johnston, L. M. Herz, H. J. Snaith, *Energy Environ. Sci.* **2014**, *7*, 982.
- [2] N.-G. Park, *Mater. Today* **2015**, *18*, 65.
- [3] L. M. Herz, *ACS Energy Lett.* **2017**, *2*, 1539.
- [4] X. Du, J. Li, G. Niu, J. H. Yuan, K. H. Xue, M. Xia, W. Pan, X. Yang, B. Zhu, J. Tang, *Nat. Commun.* **2021**, *12*, 3348.
- [5] W. Li, M. U. Rothmann, Y. Zhu, W. Chen, C. Yang, Y. Yuan, Y. Y. Choo, X. Wen, Y.-B. Cheng, U. Bach, J. Etheridge, *Nat. Energy* **2021**, *6*, 624.
- [6] H. Min, D. Y. Lee, J. Kim, G. Kim, K. S. Lee, J. Kim, M. J. Paik, Y. K. Kim, K. S. Kim, M. G. Kim, T. J. Shin, S. Il Seok, *Nature* **2021**, *598*, 444.
- [7] M. A. Green, S. P. Bremner, *Nat. Mater.* **2016**, *16*, 23.
- [8] G.-H. Kim, D. S. Kim, *Joule* **2021**, *5*, 1033.
- [9] A. Kojima, K. Teshima, Y. Shirai, T. Miyasaka, *J. Am. Chem. Soc.* **2009**, *131*, 6050.
- [10] C. Ashworth, *Nat. Rev. Mater.* **2021**, *6*, 293.
- [11] P. Meredith, A. Armin, *Nat. Commun.* **2018**, *9*, 5261.
- [12] J. J. Yoo, G. Seo, M. R. Chua, T. G. Park, Y. Lu, F. Rotermund, Y. K. Kim, C. S. Moon, N. J. Jeon, J. P. Correa-Baena, V. Bulovic, S. S. Shin, M. G. Bawendi, J. Seo, *Nature* **2021**, *590*, 587.
- [13] D. Yan, M. Liu, Z. Li, B. Hou, *J. Mater. Chem. A* **2021**, *9*, 15522.
- [14] G. H. Carey, A. L. Abdelhady, Z. Ning, S. M. Thon, O. M. Bakr, E. H. Sargent, *Chem. Rev.* **2015**, *115*, 12732.
- [15] Z. Liu, J. Yuan, S. A. Hawks, G. Shi, S.-T. Lee, W. Ma, *Sol. RRL* **2017**, *1*, 1600021.
- [16] B. Sun, A. Johnston, C. Xu, M. Wei, Z. Huang, Z. Jiang, H. Zhou, Y. Gao, Y. Dong, O. Ouellette, X. Zheng, J. Liu, M.-J. Choi, Y. Gao, S.-W. Baek, F. Laquai, O. M. Bakr, D. Ban, O. Voznyy, F. P. García De Arquer, E. H. Sargent, *Joule* **2020**, *4*, 1542.
- [17] B. Hou, B. S. Kim, H. K. H. Lee, Y. Cho, P. Giraud, M. Liu, J. Zhang, M. L. Davies, J. R. Durrant, W. C. Tsoi, Z. Li, S. D. Dimitrov, J. I. Sohn, S. Cha, J. M. Kim, *Adv. Funct. Mater.* **2020**, *30*, 2004563.
- [18] R. Hardman, *Environ. Health Perspect.* **2006**, *114*, 165.
- [19] E. Van Der Voet, R. Salminen, M. Eckelman, T. Norgate, G. Mudd, R. Hisschier, J. Spijker, M. Vijver, O. Selinus, L. Posthuma, D. De Zwart, D. Van De Meent, M. Reuter, L. Tikana, S. Valdivia, P. Wäger, M. Z. Hauschild, A. De Koning, <https://www.unep.org/resources/report/environmental-risks-and-challenges-anthropogenic-metals-flows-and-cycles> (accessed: July 2022).
- [20] A. Babayigit, H.-G. Boyen, B. Conings, *MRS Energy Sustainability* **2018**, *5*, E1.
- [21] H. Luo, P. Li, J. Ma, L. Han, Y. Zhang, Y. Song, *Adv. Energy Mater.* **2022**, *12*, 2201242.
- [22] D. Fabini, *J. Phys. Chem. Lett.* **2015**, *6*, 3546.
- [23] B. Chen, C. Fei, S. Chen, H. Gu, X. Xiao, J. Huang, *Nat. Commun.* **2021**, *12*, 5859.
- [24] N. Moody, S. Sesena, D. W. Dequillettes, B. D. Dou, R. Swartwout, J. T. Buchman, A. Johnson, U. Eze, R. Brenes, M. Johnston, C. L. Haynes, V. Bulović, M. G. Bawendi, *Joule* **2020**, *4*, 970.
- [25] X. Liu, L. Cao, Z. Guo, Y. Li, W. Gao, L. Zhou, *Materials* **2019**, *12*, 3304.
- [26] J. Li, H. L. Cao, W. B. Jiao, Q. Wang, M. Wei, I. Cantone, J. Lu, A. Abate, *Nat. Commun.* **2020**, *11*, 310.
- [27] G. Wang, Y. Zhai, S. Zhang, L. Diomedea, P. Bigini, M. Romeo, S. Cambier, S. Contal, N. H. A. Nguyen, P. Rosická, A. Ševců, C. Nickel, M. G. Vijver, W. J. G. M. Peijnenburg, *Sci. Total Environ.* **2020**, *708*, 135134.
- [28] J. I. Kwak, L. Kim, T.-Y. Lee, G. Panthi, S.-W. Jeong, S. Han, H. Chae, Y.-J. An, *Aquat. Toxicol.* **2021**, *237*, 105900.
- [29] J. I. Kwak, L. Kim, Y.-J. An, *Sci. Total Environ.* **2021**, *771*, 145388.
- [30] S.-Y. Bae, S. Y. Lee, J.-W. Kim, H. N. Umh, J. Jeong, S. Bae, J. Yi, Y. Kim, J. Choi, *Sci. Rep.* **2019**, *9*, 4242.
- [31] A. Babayigit, D. Duy Thanh, A. Ethirajan, J. Manca, M. Muller, H.-G. Boyen, B. Conings, *Sci. Rep.* **2016**, *6*, 18721.
- [32] I. R. Benmessaoud, A. L. Mahul-Mellier, E. Horvath, B. Maco, M. Spina, H. A. Lashuel, L. Forro, *Toxicol. Res.* **2016**, *5*, 407.
- [33] J.-Z. Liu, J.-S. Yang, Y.-M. Ge, Q. Yang, J.-Y. Sun, X. Yu, *Ecotoxicol. Environ. Saf.* **2021**, *208*, 111677.
- [34] Y. Zhai, Z. Wang, G. Wang, W. J. G. M. Peijnenburg, M. G. Vijver, *Chemosphere* **2020**, *249*, 126564.
- [35] D. Yan, X. Lu, S. Zhao, Z. Zhang, M. Lu, J. Feng, J. Zhang, K. Spencer, T. Watson, M. Li, B. Hou, F. Wang, Z. Li, *Sol. RRL* **2022**, *6*, 2200332.
- [36] P. Su, Y. Liu, J. Zhang, C. Chen, B. Yang, C. Zhang, X. Zhao, *J. Phys. Chem. Lett.* **2020**, *11*, 2812.
- [37] P. Wu, S. Wang, X. Li, F. Zhang, *Matter* **2022**, *5*, 1137.
- [38] M. Ren, X. Qian, Y. Chen, T. Wang, Y. Zhao, *J. Hazard. Mater.* **2022**, *426*, 127848.
- [39] J. Feng, B. Xiao, *J. Phys. Chem. Lett.* **2014**, *5*, 1278.
- [40] Z. Xiao, Z. Song, Y. Yan, *Adv. Mater.* **2019**, *31*, 1803792.
- [41] G. Xing, N. Mathews, S. Sun, S. S. Lim, Y. M. Lam, M. Grätzel, S. Mhaisalkar, T. C. Sum, *Science* **2013**, *342*, 344.
- [42] S. D. Stranks, G. E. Eperon, G. Grancini, C. Menelaou, M. J. Alcocer, T. Leijtens, L. M. Herz, A. Petrozza, H. J. Snaith, *Science* **2013**, *342*, 341.
- [43] J. Zhao, Y. Deng, H. Wei, X. Zheng, Z. Yu, Y. Shao, J. E. Shield, J. Huang, *Sci. Adv.* **2017**, *3*, ea05616.

- [44] J. T.-W. Wang, Z. Wang, S. Pathak, W. Zhang, D. W. Dequillettes, F. Wisnivesky-Rocca-Rivarola, J. Huang, P. K. Nayak, J. B. Patel, H. A. Mohd Yusof, Y. Vaynzof, R. Zhu, I. Ramirez, J. Zhang, C. Ducati, C. Grovenor, M. B. Johnston, D. S. Ginger, R. J. Nicholas, H. J. Snaith, *Energy Environ. Sci.* **2016**, *9*, 2892.
- [45] B. Saporov, D. B. Mitzi, *Chem. Rev.* **2016**, *116*, 4558.
- [46] C. Li, X. Lu, W. Ding, L. Feng, Y. Gao, Z. Guo, *Acta Crystallogr., Sect. B: Struct. Sci.* **2008**, *64*, 702.
- [47] F. Brivio, J. M. Frost, J. M. Skelton, A. J. Jackson, O. J. Weber, M. T. Weller, A. R. Goñi, A. M. A. Leguy, P. R. F. Barnes, A. Walsh, *Phys. Rev. B* **2015**, *92*, 144308.
- [48] T. Umebayashi, K. Asai, T. Kondo, A. Nakao, *Phys. Rev. B* **2003**, *67*, 155405.
- [49] W.-J. Yin, T. Shi, Y. Yan, *J. Phys. Chem. C* **2015**, *119*, 5253.
- [50] W.-J. Yin, J.-H. Yang, J. Kang, Y. Yan, S.-H. Wei, *J. Mater. Chem. A* **2015**, *3*, 8926.
- [51] I. Kang, F. W. Wise, *J. Opt. Soc. Am. B* **1997**, *14*, 1632.
- [52] M. A. Hines, G. D. Scholes, *Adv. Mater.* **2003**, *15*, 1844.
- [53] J. B. Sambur, T. Novet, B. A. Parkinson, *Science* **2010**, *330*, 63.
- [54] S. Zheng, J. Chen, E. M. J. Johansson, X. Zhang, *iScience* **2020**, *23*, 101753.
- [55] M. Yuan, M. Liu, E. H. Sargent, *Nat. Energy* **2016**, *1*, 16016.
- [56] M. Liu, Y. Chen, C. S. Tan, R. Quintero-Bermudez, A. H. Proppe, R. Munir, H. Tan, O. Voznyy, B. Scheffel, G. Walters, A. P. T. Kam, B. Sun, M. J. Choi, S. Hoogland, A. Amassian, S. O. Kelley, F. P. Garcia De Arquer, E. H. Sargent, *Nature* **2019**, *570*, 96.
- [57] M.-G. Ju, M. Chen, Y. Zhou, J. Dai, L. Ma, N. P. Padture, X. C. Zeng, *Joule* **2018**, *2*, 1231.
- [58] B. Hailegnaw, S. Kirmayer, E. Edri, G. Hodes, D. Cahen, *J. Phys. Chem. Lett.* **2015**, *6*, 1543.
- [59] J. Yang, B. D. Siempelkamp, D. Liu, T. L. Kelly, *ACS Nano* **2015**, *9*, 1955.
- [60] A. M. A. Leguy, Y. Hu, M. Campoy-Quiles, M. I. Alonso, O. J. Weber, P. Azarhoosh, M. Van Schilfgaarde, M. T. Weller, T. Bein, J. Nelson, P. Docampo, P. R. F. Barnes, *Chem. Mater.* **2015**, *27*, 3397.
- [61] J. A. Christians, P. A. Miranda Herrera, P. V. Kamat, *J. Am. Chem. Soc.* **2015**, *137*, 1530.
- [62] S.-W. Lee, S. Kim, S. Bae, K. Cho, T. Chung, L. E. Mundt, S. Lee, S. Park, H. Park, M. C. Schubert, S. W. Glunz, Y. Ko, Y. Jun, Y. Kang, H.-S. Lee, D. Kim, *Sci. Rep.* **2016**, *6*, 38150.
- [63] N. Aristidou, I. Sanchez-Molina, T. Chotchuangchutchaval, M. Brown, L. Martinez, T. Rath, S. A. Haque, *Angew. Chem., Int. Ed. Engl.* **2015**, *54*, 8208.
- [64] M. Liu, X. Huang, Y. Song, J. Tang, J. Cao, X. Zhang, Q. Zhang, S. Wang, T. Xu, L. Kang, X. Cai, H. Zhang, F. Yang, H. Wang, J. Z. Yu, A. K. H. Lau, L. He, X. Huang, L. Duan, A. Ding, L. Xue, J. Gao, B. Liu, T. Zhu, *Proc. Natl. Acad. Sci.* **2019**, *116*, 7760.
- [65] Y. Yu, Y. Hong, P. Gao, M. K. Nazeeruddin, *Anal. Chem.* **2016**, *88*, 12316.
- [66] J. Wan, X. Yu, J. Zou, K. Li, L. Chen, Y. Peng, Y.-B. Cheng, *Sol. Energy* **2021**, *226*, 85.
- [67] Y. Jiang, L. Qiu, E. J. Juarez-Perez, L. K. Ono, Z. Hu, Z. Liu, Z. Wu, L. Meng, Q. Wang, Y. Qi, *Nat. Energy* **2019**, *4*, 585.
- [68] A. K. Jena, Y. Numata, M. Ikegami, T. Miyasaka, *J. Mater. Chem. A* **2018**, *6*, 2219.
- [69] N. Ahn, K. Kwak, M. S. Jang, H. Yoon, B. Y. Lee, J. K. Lee, P. V. Pikhitsa, J. Byun, M. Choi, *Nat. Commun.* **2016**, *7*, 13422.
- [70] Y. Chen, H. Zhou, *J. Appl. Phys.* **2020**, *128*, 060903.
- [71] W. Chen, R. Guo, H. Tang, K. S. Wienhold, N. Li, Z. Jiang, J. Tang, X. Jiang, L. P. Kreuzer, H. Liu, M. Schwartzkopf, X. W. Sun, S. V. Roth, K. Wang, B. Xu, P. Müller-Buschbaum, *Energy Environ. Sci.* **2021**, *14*, 3420.
- [72] N. Moody, D. Yoon, A. Johnson, E. Wassweiler, M. Nasilowski, V. Bulović, M. G. Bawendi, *Adv. Sustainable Syst.* **2019**, *3*, 1900061.
- [73] K. Praeynsaert, S. J. Soenen, B. B. Manshian, S. H. Doak, K. Braeckmans, S. C. De Smedt, K. Remaut, *Acta Biomater.* **2017**, *48*, 195.
- [74] G. Panthi, R. Bajagain, Y.-J. An, S.-W. Jeong, *Process Saf. Environ. Prot.* **2021**, *149*, 115.
- [75] F. Schmidt, L. Ledermann, A. Schäffer, H. J. Snaith, M. Lenz, *J. Hazard. Mater.* **2022**, *436*, 128995.
- [76] B. Conings, A. Babayigit, H.-G. Boyen, *ACS Energy Lett.* **2019**, *4*, 873.
- [77] Y. G. Yoo, J. Park, H. N. Umh, S. Y. Lee, S. Bae, Y. H. Kim, S. E. Jerng, Y. Kim, J. Yi, *J. Ind. Eng. Chem.* **2019**, *70*, 453.
- [78] A. L. Wani, A. Ara, J. A. Usmani, *Interdiscip. Toxicol.* **2015**, *8*, 55.
- [79] A. Babayigit, A. Ethirajan, M. Muller, B. Conings, *Nat. Mater.* **2016**, *15*, 247.
- [80] H. Needleman, *Annu. Rev. Med.* **2004**, *55*, 209.
- [81] L. Truong, I. S. Moody, D. P. Stankus, J. A. Nason, M. C. Lonergan, R. L. Tanguay, *Arch. Toxicol.* **2011**, *85*, 787.
- [82] Y. Chang, K. Li, Y. Feng, N. Liu, Y. Cheng, X. Sun, Y. Feng, X. Li, Z. Wu, H. Zhang, *Nano Res.* **2016**, *9*, 3812.
- [83] J. H. Kim, H. R. Kim, B. R. Lee, E. S. Choi, S. I. In, E. Kim, *Int. J. Nanomed.* **2015**, *10*, 5513.
- [84] Y. Cao, H. Liu, Q. Li, Q. Wang, W. Zhang, Y. Chen, D. Wang, Y. Cai, *J. Inorg. Biochem.* **2013**, *126*, 70.
- [85] Q. Li, X. Hu, Y. Bai, M. Alattar, D. Ma, Y. Cao, Y. Hao, L. Wang, C. Jiang, *Food Chem. Toxicol.* **2013**, *60*, 213.
- [86] J. Jeong, M. Kim, J. Seo, H. Lu, P. Ahlawat, A. Mishra, Y. Yang, M. A. Hope, F. T. Eickemeyer, M. Kim, Y. J. Yoon, I. W. Choi, B. P. Darwich, S. J. Choi, Y. Jo, J. H. Lee, B. Walker, S. M. Zakeeruddin, L. Emsley, U. Rothlisberger, A. Hagfeldt, D. S. Kim, M. Grätzel, J. Y. Kim, *Nature* **2021**, *592*, 381.
- [87] J. Dagar, M. Fenske, A. Al-Ashouri, C. Schultz, B. Li, H. Köbler, R. Munir, G. Parmasivam, J. Li, I. Levine, A. Merdasa, L. Kegelmann, H. Näsström, J. A. Marquez, T. Unold, D. M. Töbrens, R. Schlattmann, B. Stegemann, A. Abate, S. Albrecht, E. Unger, *ACS Appl. Mater. Interfaces* **2021**, *13*, 13022.
- [88] A. Abate, *Joule* **2017**, *1*, 659.
- [89] C. Walkons, R. Murshed, S. Bansal, *Sol. RRL* **2020**, *4*, 2000299.
- [90] S. Attique, N. Ali, S. Rauf, S. Ali, A. Khesro, R. Khatoon, E. U. Khan, F. Akram, S. Yang, H. Wu, *Sol. RRL* **2021**, *5*, 2100212.
- [91] L. Liang, P. Gao, *Adv. Sci.* **2018**, *5*, 1700331.
- [92] F. Giustino, H. J. Snaith, *ACS Energy Lett.* **2016**, *1*, 1233.
- [93] I. Kopacic, B. Friesenbichler, S. F. Hoeffler, B. Kunert, H. Plank, T. Rath, G. Trimmel, *Acs Appl. Energy Mater.* **2018**, *1*, 343.
- [94] F. Gu, Z. Zhao, C. Wang, H. Rao, B. Zhao, Z. Liu, Z. Bian, C. Huang, *Sol. RRL* **2019**, *3*, 1900213.
- [95] W. Shockley, H. J. Queisser, *J. Appl. Phys.* **1961**, *32*, 510.
- [96] B.-B. Yu, Z. Chen, Y. Zhu, Y. Wang, B. Han, G. Chen, X. Zhang, Z. Du, Z. He, *Adv. Mater.* **2021**, *33*, 2102055.
- [97] J. Cao, F. Yan, *Energy Environ. Sci.* **2021**, *14*, 1286.
- [98] G. Wang, J. Chang, J. Bi, M. Lei, C. Wang, Q. Qiao, *Sol. RRL* **2022**, *6*, 2100841.
- [99] T. Ye, X. Wang, K. Wang, S. Ma, D. Yang, Y. Hou, J. Yoon, K. Wang, S. Priya, *ACS Energy Lett.* **2021**, *6*, 1480.
- [100] L. Lanzetta, J. M. Marin-Beloqui, I. Sanchez-Molina, D. Ding, S. A. Haque, *ACS Energy Lett.* **2017**, *2*, 1662.
- [101] L. Lanzetta, N. Aristidou, S. A. Haque, *J. Phys. Chem. Lett.* **2020**, *11*, 574.
- [102] Y. Li, W. Sun, W. Yan, S. Ye, H. Rao, H. Peng, Z. Zhao, Z. Bian, Z. Liu, H. Zhou, C. Huang, *Adv. Energy Mater.* **2016**, *6*, 1601353.

- [103] X. Lian, J. Chen, Y. Zhang, M. Qin, J. Li, S. Tian, W. Yang, X. Lu, G. Wu, H. Chen, *Adv. Funct. Mater.* **2019**, *29*, 1807024.
- [104] M. Li, Z. Wang, M. Zhuo, Y. Hu, K. Hu, Q. Ye, S. M. Jain, Y. Yang, X. Gao, L. Liao, *Adv. Mater.* **2018**, *30*, e1800258.
- [105] H. Tang, Y. Shang, W. Zhou, Z. Peng, Z. Ning, *Sol. RRL* **2019**, *3*, 1800256.
- [106] Z. Zhang, J. Liang, Y. Zheng, X. Wu, J. Wang, Y. Huang, Y. Yang, Z. Zhou, L. Wang, L. Kong, K. M. Reddy, C. Qin, C.-C. Chen, *J. Mater. Chem. A* **2021**, *9*, 17830.
- [107] M. Li, W. Zuo, Y. Yang, M. H. Aldamasy, Q. Wang, S. H. T. Cruz, S. Feng, M. Saliba, Z. Wang, A. Abate, *ACS Energy Lett.* **2020**, *5*, 1923.
- [108] L. Gollino, T. Pauporté, *Sol. RRL* **2021**, *5*, 2000616.
- [109] E. Horváth, M. Kollár, P. Andričević, L. Rossi, X. Mettan, L. Forró, *ACS Appl. Mater. Interfaces* **2021**, *13*, 33995.
- [110] B. Niu, H. Wu, J. Yin, B. Wang, G. Wu, X. Kong, B. Yan, J. Yao, C.-Z. Li, H. Chen, *ACS Energy Lett.* **2021**, *6*, 3443.
- [111] S. Chen, Y. Deng, X. Xiao, S. Xu, P. N. Rudd, J. Huang, *Nat. Sustainable* **2021**, *4*, 636.
- [112] Y. Hu, Z. He, X. Jia, S. Zhang, Y. Tang, J. Wang, M. Wang, G. Sun, G. Yuan, L. Han, *Small Methods* **2022**, *6*, 2101257.
- [113] Y. Liang, P. Song, H. Tian, C. Tian, W. Tian, Z. Nan, Y. Cai, P. Yang, C. Sun, J. Chen, L. Xie, Q. Zhang, Z. Wei, *Adv. Funct. Mater.* **2022**, *32*, 2110139.
- [114] X. Li, J. Du, H. Duan, H. Wang, L. Fan, Y. Sun, Y. Sui, J. Yang, F. Wang, L. Yang, *Nano Res.* **2022**, *15*, 1375.
- [115] Q. Cao, T. Wang, J. Yang, Y. Zhang, Y. Li, X. Pu, J. Zhao, H. Chen, X. Li, I. Tojiboyev, J. Chen, L. Etgar, X. Li, *Adv. Funct. Mater.* **2022**, *32*, 2201036.
- [116] J. Lee, G.-W. Kim, M. Kim, S. A. Park, T. Park, *Adv. Energy Mater.* **2020**, *10*, 1902662.
- [117] Y. Dong, J. Zhang, Y. Yang, J. Wang, B. Hu, W. Wang, W. Cao, S. Gai, D. Xia, K. Lin, R. Fan, *Nano Energy* **2022**, *97*, 107184.
- [118] S. Chen, Y. Deng, H. Gu, S. Xu, S. Wang, Z. Yu, V. Blum, J. Huang, *Nat. Energy* **2020**, *5*, 1003.
- [119] H. Wang, H. Liu, W. Li, L. Zhu, H. Chen, *Nano Energy* **2020**, *77*, 105160.
- [120] Z. Ku, Y. Rong, M. Xu, T. Liu, H. Han, *Sci. Rep.* **2013**, *3*, 3132.
- [121] J. Wang, R. Zhang, H. Xu, Y. Chen, H. Zhang, N.-G. Park, *ACS Energy Lett.* **2022**, *7*, 1577.
- [122] S. Shao, M. A. Loi, *Adv. Mater. Interfaces* **2020**, *7*, 1901469.
- [123] P. Yan, J. Cao, J. Pang, Z. Yang, X. Wang, X. Yao, *Org. Electron.* **2021**, *93*, 106158.
- [124] C. Li, L. Wang, P.-J. Yan, H. Liu, J. Cao, C.-C. Chen, Y. Tang, *Chem. Eng. J.* **2021**, *409*, 128167.
- [125] G.-B. Xiao, L.-Y. Wang, X.-J. Mu, X.-X. Zou, Y.-Y. Wu, J. Cao, *CCS Chem.* **2021**, *3*, 25.
- [126] H. Liang, W. D. Wang, S. Mai, X. Lv, J. Fang, J. Cao, *Chem. Eng. J.* **2022**, *429*, 132405.
- [127] Y. Hu, W. Song, X. Wang, X. Shi, X. Jia, Z. He, S. Zhang, G. Yuan, M. Wang, J. Wang, G. Sun, T. Sun, Y. Tang, *Chem. Eng. J.* **2022**, *433*, 134566.
- [128] Q. Wang, Z. Lin, J. Su, Y. Xu, X. Guo, Y. Li, M. Zhang, J. Zhang, J. Chang, Y. Hao, *EcoMat* **2022**, *4*, e12185.
- [129] X. Wei, M. Xiao, B. Wang, C. Wang, Y. Li, J. Dou, Z. Cui, J. Dou, H. Wang, S. Ma, C. Zhu, G. Yuan, N. Yang, T. Song, H. Zhou, H. Chen, Y. Bai, Q. Chen, *Angew. Chem., Int. Ed.* **2022**, *61*, e202204314.
- [130] X. Zhu, H. Dong, J. Chen, J. Xu, Z. Li, F. Yuan, J. Dai, B. Jiao, X. Hou, J. Xi, Z. Wu, *Adv. Funct. Mater.* **2022**, *32*, 2202408.
- [131] X. Meng, X. Hu, Y. Zhang, Z. Huang, Z. Xing, C. Gong, L. Rao, H. Wang, F. Wang, T. Hu, L. Tan, Y. Song, Y. Chen, *Adv. Funct. Mater.* **2021**, *31*, 2106460.
- [132] M. Z. Mokhtar, J. He, M. Li, Q. Chen, J. C. R. Ke, D. J. Lewis, A. G. Thomas, B. F. Spencer, S. A. Haque, B. R. Saunders, *Chem. Commun.* **2021**, *57*, 994.
- [133] J. Zhang, R. Li, S. Aperi, P. Wang, B. Shi, J. Jiang, N. Ren, W. Han, Q. Huang, G. Brocks, Y. Zhao, S. Tao, X. Zhang, *Sol. RRL* **2021**, *5*, 2100464.
- [134] B. Wang, J. Ma, Z. Li, G. Chen, Q. Gu, S. Chen, Y. Zhang, Y. Song, J. Chen, X. Pi, X. Yu, D. Yang, *Nano Res.* **2022**, *15*, 1069.
- [135] D. Xu, R. Mai, Y. Jiang, C. Chen, R. Wang, Z. Xu, K. Kempa, G. Zhou, J.-M. Liu, J. Gao, *Energy Environ. Sci.* **2022**, *15*, 3891.
- [136] S. Wu, Z. Li, M. Q. Li, Y. Diao, F. Lin, T. Liu, J. Zhang, P. Tieu, W. Gao, F. Qi, X. Pan, Z. Xu, Z. Zhu, A. K. Jen, *Nat. Nanotechnol.* **2020**, *15*, 934.
- [137] H. Zhang, K. Li, M. Sun, F. Wang, H. Wang, A. K.-Y. Jen, *Adv. Energy Mater.* **2021**, *11*, 2102281.
- [138] X. Li, F. Zhang, H. He, J. J. Berry, K. Zhu, T. Xu, *Nature* **2020**, *578*, 555.
- [139] X. Li, F. Zhang, J. Wang, J. Tong, T. Xu, K. Zhu, *Nat. Sustainable* **2021**, *4*, 1038.
- [140] X. Xiao, M. Wang, S. Chen, Y. Zhang, H. Gu, Y. Deng, G. Yang, C. Fei, B. Chen, Y. Lin, M. D. Dickey, J. Huang, *Sci. Adv.* **2021**, *7*, eabi8249.
- [141] Z. Li, X. Wu, B. Li, S. Zhang, D. Gao, Y. Liu, X. Li, N. Zhang, X. Hu, C. Zhi, A. K.-Y. Jen, Z. Zhu, *Adv. Energy Mater.* **2022**, *12*, 2103236.
- [142] Z. Li, X. Wu, S. Wu, D. Gao, H. Dong, F. Huang, X. Hu, A. K. Y. Jen, Z. Zhu, *Nano Energy* **2022**, *93*, 106853.
- [143] Z. Wang, M. Tang, *Environ. Res.* **2021**, *194*, 110593.
- [144] D. Benito-Alifonso, S. Tremel, B. Hou, H. Lockyear, J. Mantell, D. J. Fermin, P. Verkade, M. Berry, M. C. Galan, *Angew. Chem., Int. Ed.* **2014**, *53*, 810.
- [145] A. R. C. Osypiw, S. Lee, S.-M. Jung, S. Leoni, P. M. Smowton, B. Hou, J. M. Kim, G. A. J. Amaratunga, *Mater. Adv.* **2022**, *3*, 6773.
- [146] A. Hoshino, K. Fujioka, T. Oku, M. Suga, Y. F. Sasaki, T. Ohta, M. Yasuhara, K. Suzuki, K. Yamamoto, *Nano Lett.* **2004**, *4*, 2163.
- [147] J. E. Boercker, D. L. Woodall, P. D. Cunningham, D. Placencia, C. T. Ellis, M. H. Stewart, T. H. Brintlinger, R. M. Stroud, J. G. Tischler, *Chem. Mater.* **2018**, *30*, 4112.
- [148] C. B. M. And, C. R. Kagan, M. G. Bawendi, *Annu. Rev. Mater. Sci.* **2000**, *30*, 545.
- [149] B. Hou, Y. Cho, B. S. Kim, J. Hong, J. B. Park, S. J. Ahn, J. I. Sohn, S. Cha, J. M. Kim, *ACS Energy Lett.* **2016**, *1*, 834.
- [150] R. Wang, Y. Shang, P. Kanjanaboos, W. Zhou, Z. Ning, E. H. Sargent, *Energy Environ. Sci.* **2016**, *9*, 1130.
- [151] J.-A. Alberola-Borràs, R. Vidal, E. J. Juárez-Pérez, E. Mas-Marzá, A. Guerrero, I. Mora-Seró, *Sol. Energy Mater. Sol. Cells* **2018**, *179*, 169.
- [152] C. G. Poll, G. W. Nelson, D. M. Pickup, A. V. Chadwick, D. J. Riley, D. J. Payne, *Green Chem.* **2016**, *18*, 2946.
- [153] J. M. Kadro, N. Pellet, F. Giordano, A. Ulianov, O. Müntener, J. Maier, M. Grätzel, A. Hagfeldt, *Energy Environ. Sci.* **2016**, *9*, 3172.
- [154] A. Binek, M. L. Petrus, N. Huber, H. Bristow, Y. Hu, T. Bein, P. Docampo, *ACS Appl. Mater. Interfaces* **2016**, *8*, 12881.
- [155] X. Feng, Q. Guo, J. Xiu, Z. Ying, K. W. Ng, L. Huang, S. Wang, H. Pan, Z. Tang, Z. He, *Cell Rep. Phys. Sci.* **2021**, *2*, 100341.
- [156] S. Y. Park, J.-S. Park, B. J. Kim, H. Lee, A. Walsh, K. Zhu, D. H. Kim, H. S. Jung, *Nat. Sustainable* **2020**, *3*, 1044.
- [157] J. S. Hong, H. J. Kim, C. H. Sohn, O. Y. Gong, J. H. Choi, K. H. Cho, G. S. Han, K. T. Nam, H. S. Jung, *Energy Environ. Mater.* **2022**, <https://doi.org/10.1002/eem2.12374>.
- [158] J. Xu, Z. Hu, L. Huang, X. Huang, X. Jia, J. Zhang, J. Zhang, Y. Zhu, *Prog. Photovoltaics Res. Appl.* **2017**, *25*, 1022.
- [159] Y.-Y. Huang, G. Gollavelli, Y.-H. Chao, C.-S. Hsu, *J. Mater. Chem. C* **2016**, *4*, 7595.

- [160] L. Hong, Y. Hu, A. Mei, Y. Sheng, P. Jiang, C. Tian, Y. Rong, H. Han, *Adv. Funct. Mater.* **2017**, *27*, 1703060.
- [161] P. Chhillar, B. P. Dharamaniya, V. Dutta, S. K. Pathak, *ACS Omega* **2019**, *4*, 11880.
- [162] S. Zhang, L. Shen, M. Huang, Y. Yu, L. Lei, J. Shao, Q. Zhao, Z. Wu, J. Wang, S. Yang, *ACS Sustainable Chem. Eng.* **2018**, *6*, 7558.
- [163] M. Ren, Y. Miao, T. Zhang, Z. Qin, Y. Chen, N. Wei, X. Qian, T. Wang, Y. Zhao, *ACS Sustainable Chem. Eng.* **2021**, *9*, 16519.
- [164] K. Wang, T. Ye, X. Huang, Y. Hou, J. Yoon, D. Yang, X. Hu, X. Jiang, C. Wu, G. Zhou, S. Priya, *Matter* **2021**, *4*, 2522.
- [165] X. Tian, S. D. Stranks, F. You, *Sci. Adv.* **2020**, *6*, eabb0055.



**Xingwen Lu** is an associate professor in environmental engineering at the School of Environmental Science and Engineering, Guangdong University of Technology. She received her Ph.D. degree from the Department of Civil Engineering at the University of Hong Kong in 2013, and worked as a post-doc at the University of Hong Kong (2013–2015). Her main research interest includes valuable metal recovery from e-wastes, phosphorus recycling from wastewater, and the fate and transformation of hazardous metal in waste streams.



**Dong Yan** is a lecturer at the School of Physics and Optoelectronic Engineering, Foshan University, China. She is also a visiting research scholar in the School of Engineering and Materials Science at Queen Mary University of London, UK. She obtained her Ph.D. degree from the Institute of Microelectronics, Chinese Academy of Sciences in 2016. Her research interests include stability and toxicity study of perovskite and quantum dot solar cells and device characterization.



**Jiangtao Feng** is an associate professor in Environmental Engineering at the School of Energy and Power Engineering, Xi'an Jiaotong University. He received his Ph.D. degree from Xi'an Jiaotong University in 2011. His main research interest includes the adsorption of organic pollutants and heavy metal ions in water, advanced treatment and recycling of sewage, new environmental adsorption materials, and photocathode protection materials.



**Meng Li** obtained his Ph.D. degree in materials science and engineering under the supervision of Prof. Liang-Sheng Liao from Soochow University in June 2018. He pursued his postdoctoral research in the Helmholtz-Zentrum Berlin für Materialien und Energie (HZB) from October 2018 to September 2021. Currently, he joined the Key Lab for Special Functional Materials of Ministry of Education, Henan University. Dr. Li's group conducts research on organic–inorganic hybrid materials for optoelectronic applications. His main research interests lie in the application of nontoxic photovoltaic and luminescent materials and devices.



**Bo Hou** is a senior lecturer in the School of Physics and Astronomy, at Cardiff University. He received his Ph.D. degree from the University of Bristol (2010–2014). He worked as a postdoctoral researcher at the University of Oxford (2014–2018, Wolfson College) and a senior research fellow at the University of Cambridge (2018–2020, St Edmund's College). His research interests include quantum dot synthesis, quantum dot solar cells, quantum dot optoelectronics, transmission electron microscopy, and dynamic charge transfer analysis in energy devices.



**Zhe Li** is a senior lecturer in Materials Science at the School of Engineering and Materials Science, Queen Mary University of London. He received his Ph.D. degree from Cavendish Laboratory at the University of Cambridge in 2012, and worked as a research associate/research fellow/junior group leader at Imperial College London (2012–2015) and Swansea University (2015–2017) and as a Lecturer of Energy Materials at School of Engineering, Cardiff University (2018–2019). His main research interest includes organic, perovskite, and quantum dot photovoltaic cells, including emerging target applications, stability analysis, and advanced materials, and device characterization.



**Fei Wang** is an associate professor in environmental science at the School of Environment, Jinan University. He received his Ph.D. degree from the University of Hong Kong in 2013, and worked as a post-doc at the University of Hong Kong (2013–2015). His main research interest includes the environmental effects of organic pollutants and heavy metals, the recovery of valuable metals from lithium-ion batteries, and environmental health and human exposure.